Six-dimensional muon beam cooling using a homogeneous absorber; Concepts, beam dynamics, cooling decrements, and equilibrium emittances in a helical dipole channel

Yaroslav Derbenev

Thomas Jefferson National Accelerator Facility, Newport News, VA 23606

Rolland P. Johnson*

Muons, Inc. Batavia, IL 60510

The fast reduction of the six-dimensional phase space of muon beams is an essential requirement for muon colliders and also of great importance for neutrino factories based on accelerated muon beams. Ionization cooling, where all momentum components are degraded by an energy absorbing material and only the longitudinal momentum is restored by rf cavities, provides a means to quickly reduce transverse beam sizes. However, the beam energy spread cannot be reduced by this method unless the longitudinal emittance can be transformed or exchanged into the transverse emittance. Emittance exchange plans until now have been accomplished by using magnets to disperse the beam along the face of a wedge-shaped absorber such that higher momentum particles pass through thicker parts of the absorber and thus suffer larger ionization energy loss. In the scheme advocated in this paper, a special magnetic channel designed such that higher momentum corresponds to a longer path length, and therefore larger ionization energy loss, provides the desired emittance exchange in a homogeneous absorber without special edge shaping. Normal-conducting rf cavities imbedded in the magnetic field regenerate the energy lost in the absorber. One very attractive example of a cooling channel based on this principle uses a series of high-gradient rf cavities filled with dense hydrogen gas, where the cavities are in a magnetic channel composed of a solenoidal

* Corresponding author. Email address rol@muonsinc.com.

field with superimposed helical transverse dipole and quadrupole fields. In this scheme, the energy loss, the rf energy regeneration, the emittance exchange, and the transverse cooling happen simultaneously. The theory of this helical channel is described in some detail to support the analytical prediction of almost a factor of a million reduction in six-dimensional phase space volume in a channel about 56 meters long. Equations describing the particle beam dynamics are derived and beam stability conditions are explored. Equations describing six-dimensional cooling in this channel are also derived, including explicit expressions for cooling decrements and equilibrium emittances.

PACS **29.27.-a, 29.20. Dh, 14.60.Ef, 41.85.Lc**

Table of Contents

I. INTRODUCTION

The fast reduction of the six-dimensional (6D) phase space of muon beams is an essential requirement for muon colliders [1,2,3] and also of great importance for neutrino factories [4,5,6] based on accelerated muon beams. Ionization cooling [7,8] provides a means to quickly reduce transverse beam sizes, but the beam momentum spread cannot be reduced by this method unless the longitudinal emittance can be transformed or exchanged into the transverse emittance.

In the scheme advocated in this paper, a muon beam cooling-channel is made of a series of rf cavities filled with high-density hydrogen gas, which provides simultaneous emittance exchange and transverse ionization cooling by virtue of a superimposed helical magnetic field. Coils placed outside of the rf cavities create a solenoidal magnetic field component, which does not change direction, and transverse dipole and quadrupole helical components, which change direction along the channel axis in the same manner as is found in spin-rotating magnets used in Siberian Snakes [9]. The energy loss, the rf energy regeneration, the emittance exchange, and the transverse cooling happen simultaneously. Except for the pressure windows at the two ends of the channel, the muons pass only through hydrogen for the most efficient cooling possible. As the beam travels down the channel the beam bunches become shorter and smaller such that higher frequency rf cavities with smaller transverse dimensions can be used to allow more efficient rf parameters and smaller diameter magnets to enable higher fields and gradients.

A. Emittance exchange in a homogeneous absorber

The idea that is the basis of this paper for a 6D cooling-channel is seen in a comparison of figures 1a and 1b. Figure 1a is a conceptual picture of the usual mechanism for reducing the energy spread in a muon beam. The dispersion of the beam generated by the dipole magnet in figure 1a creates an energy-position correlation at a wedge-shaped absorber. Higher energy particles

pass through thicker parts of the absorber and so have more energy loss than particles of less energy. After the absorber the beam becomes more monoenergetic. This process is emittance exchange, as it is sometimes called, because the transverse emittance must grow to allow the longitudinal emittance to be cooled. In figure 1a, the beam is in vacuum except in the wedge absorber. Subsequent rf cavities, also in vacuum, replace the energy lost in the absorber. The process is limited by multiple scattering in the absorber and the high-Z windows that isolate the evacuated rf cavities and that contain the absorbers.

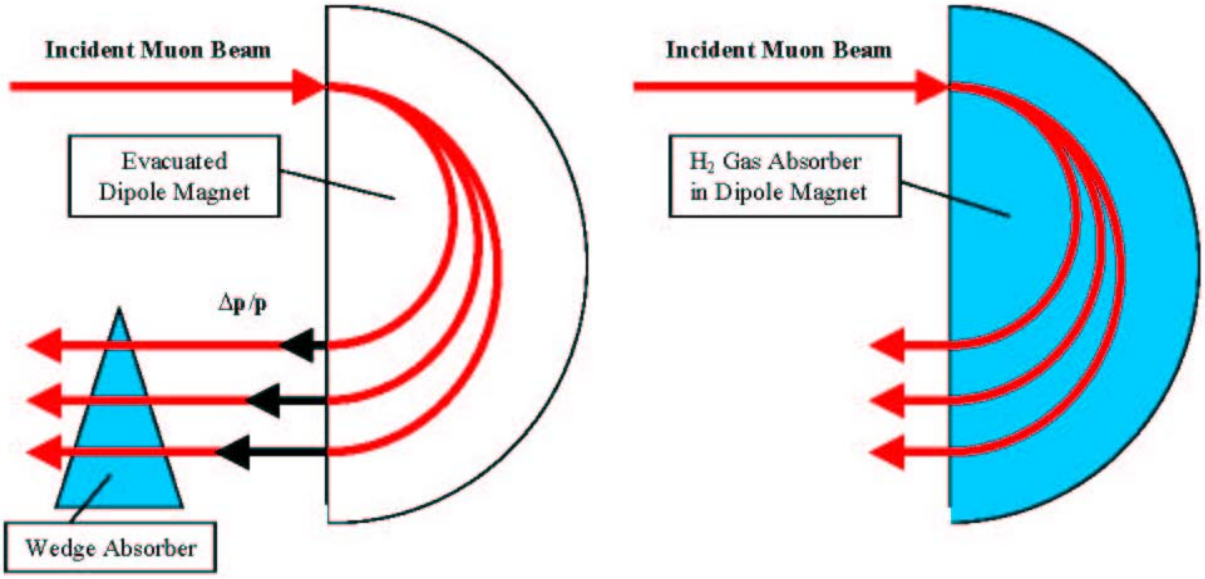

FIG. 1. (Color) a) Wedge Absorber Technique b) New Homogeneous Absorber Technique.

In previous cooling plans, both the emittance exchange process and the transverse ionization beam cooling processes have been implemented by sequentially alternating absorbers and evacuated rf cavities. Moreover, the usual 6D schemes require sequential use of wedge absorbers for emittance exchange followed by unshaped absorbers for transverse cooling followed by rf cavities to regenerate the lost energy.

The new idea advocated in this paper is shown conceptually in Fig. 1b. In this simpler picture, the cooling channel magnets are filled with dense gaseous energy absorber. The magnetic dispersion creates a longer path length for particles of higher momentum. The longer path length, in turn, times the absorber dE/ds gives the energy loss correlation with momentum needed for 6D cooling. Thus a homogeneous absorber, without shaped edges, can be used to accomplish emittance exchange. Note that the 180-degree geometry shown in the figures is chosen purely to illustrate the principles involved; the geometry of the cooling channel proposed below is quite different.

A second new idea advocated here is that the rf cavities can be inside the cooling channel magnets and operate while filled with the gaseous energy absorber. Thus the ionization energy loss and the rf energy regeneration can be simultaneous rather than sequential.

B. rf cavities filled with absorber

The initial concept that a homogeneous absorber, one without shaped edges, would be attractive for emittance exchange is related to the development of rf cavities filled with dense gas [10]. A project [11] presently underway at Fermilab has demonstrated that an 800 MHz rf cell filled with cold, pressurized hydrogen gas can achieve 80 MV/m with exceptionally short conditioning times [12]. This project is to study the use of high-pressure gases in rf cavities to facilitate large gradients by suppressing high-voltage breakdown by virtue of Paschen's Law [13]. A series of contiguous pillbox cavities similar to the one being developed in this project could define the helical cooling channel described in this paper.

Most rf cavities associated with particle accelerators operate in as close to a vacuum as possible to avoid electrical breakdown. This is done so that electrons or ions that are accelerated by the high voltages in the rf cavity rarely encounter atoms of the residual gas, and so the avalanche process of breakdown is inhibited. Other rf systems that do not require the ultrahigh vacuum of an

accelerator typically suppress rf breakdown by using dense materials between electrodes. Ions passing through these materials, which include high-pressure and/or high-density gases, have such a short mean free path between collisions that they do not accelerate to energies high enough to create an avalanche. The relationship between the electrical breakdown voltage and the product of gas pressure and gap width is known as Paschen's Law.

The gas in the cavities also acts as the energy absorber needed for ionization cooling, where hydrogen or helium are the only realistic choices because of their favorable energy loss and radiation length. All things considered, however, hydrogen is superior in all aspects except for perceived safety concerns. Hydrogen gas has over twice the ionization cooling effectiveness as helium in that it allows a final cooled emittance (proportional to $(Z+1)$), that is smaller by a factor of 1.5 in each transverse plane. At the same pressure, hydrogen suppresses rf breakdown at a voltage that is six times higher than helium. Hydrogen is also superior in heat capacity and viscosity, which are important parameters for the engineering of a practical cooling channel.

This idea of filling rf cavities with gas is new for particle accelerators and is only possible for muons because they do not scatter as do strongly interacting protons or shower electro-magnetically as do less-massive electrons. Additionally, use of a gaseous absorber presents other practical advantages that make it a simpler and more effective cooling method compared to liquid hydrogen flasks in the conventional designs of transverse cooling channels, such as the scheme envisioned by the MICE [14] collaboration for a demonstration experiment proposed for Rutherford Appleton Laboratory (RAL).

C. Helical Cooling Channel Segment Example

Figure 2 is a display from G4Beamline [15], a simulation program based on GEANT4 [16], of an initial 10 meter-long cooling channel segment, which shows one possible arrangement of

pressurized rf cavities. In this example, the rf cavities are displaced transversely from the structure axis such that the muon beam passes through their centers. The forty rf cavities shown in red in this example are 200 MHz pillbox cavities with 30 cm diameter aperture. Figure 3 is an end-view of the same channel, where the (red) outlines of the rf cavities can be seen. Fifty muon trajectories (blue) are seen relative to the (white) equilibrium orbit.

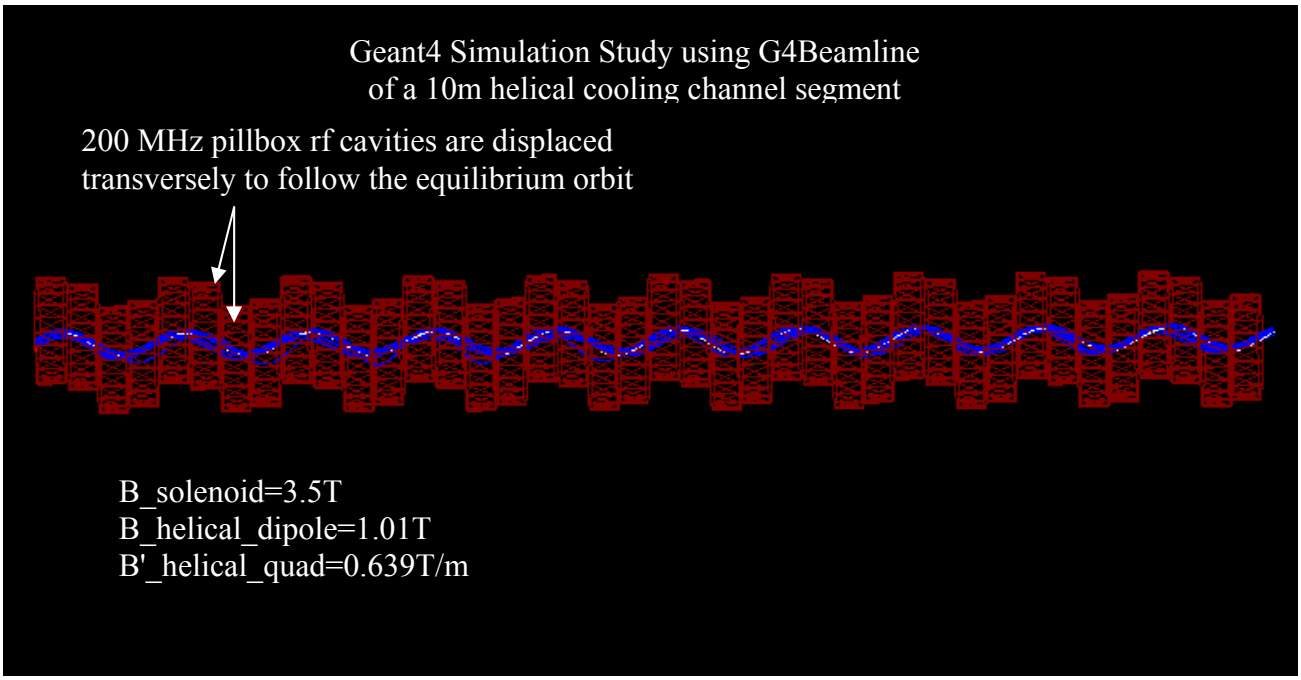

FIG 2. (Color) G4Beamline display of a 10 meter-long segment of a helical cooling channel that is being simulated. The outlines of the forty 200 MHz pillbox rf cavities are shown in red. In this simulation, superimposed magnetic fields with solenoidal and helical components provide focusing and dispersion as the muons pass through the hydrogen-filled rf cavities. Muon trajectories are shown (blue) as they oscillate about the equilibrium orbit (white).

Superconducting coils (not shown) surround the rf cavities to provide a magnetic field with solenoidal, helical dipole, and helical quadrupole components to create the muon orbits indicated by the blue traces in the figure. The object of this paper is to describe the characteristics of this magnetic channel, which has unusually good acceptance and cooling qualities. The simulations of

this channel are underway and will be reported in later papers. Later in this paper, a cooling channel example is described which has three segments such as the one shown here, each with rf frequencies and dimensions adjusted as the beam shrinks to attain optimum cooling rates.

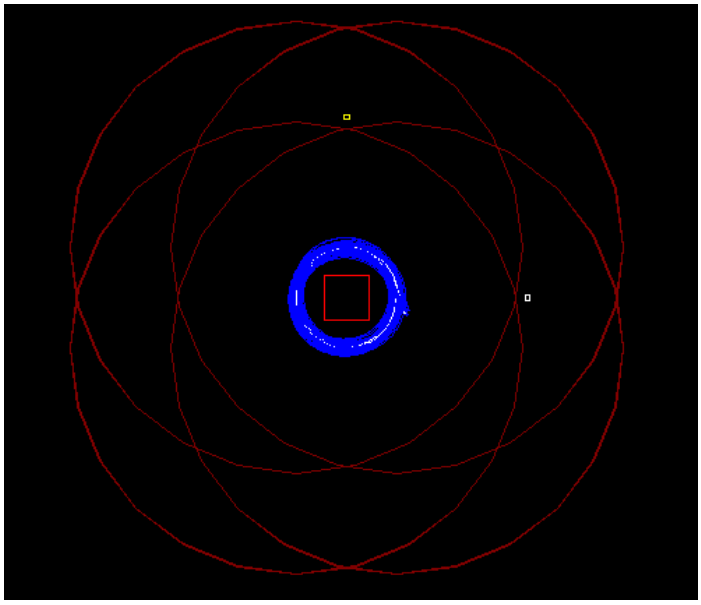

FIG 3. (Color) The same as conditions as figure 2, but viewed looking down the cooling channel. The beam here is at 200 MeV/c with a helix radius of 11 cm. The outlines of the radially-displaced rf cavities are shown in red. The red box shown for orientation in the center is 10 cm on a side.

D. Comparison with Ring Coolers

There have been several proposed emittance exchange schemes based on the use of wedge absorbers in muon beam accelerators and storage rings [1, 2, 17]. The most recent progress in the study of 6D cooling has been with Ring Coolers (RC), where muons pass several times through a small storage ring with dispersion regions for emittance exchange cooling [18]. RCs are sophisticated devices, where many difficult problems have been addressed using

combinations of dipole, solenoidal, and quadrupole magnets interspersed with rf cavities and energy absorbers of different materials and shapes.

Although 6D cooling is very much required to satisfy the requirements of a muon collider, in the most recent exercises it is looked at more often as a possible way to economize the construction costs of a neutrino factory. In this context, 6D cooling reduces transverse beam sizes and bunch lengths so that higher frequency and therefore more economical rf can accelerate muons to the energy of the storage ring of a neutrino factory. This acceleration to the storage ring energy in Fermilab and Brookhaven neutrino factory design studies used recirculating Linacs, which amounted to more than a quarter of the neutrino factory construction costs.

An RC is in itself a way to economize in that the 15 or so turns the beam makes during the cooling process allows equipment to be reused. A ring is also a rather familiar device for accelerator physicists, where tricks for dispersion creation and simultaneous matching of transverse and longitudinal constraints are known.

All RCs share common difficulties. Injection (and extraction to a lesser extent) is particularly troublesome because it requires a kicker magnet with parameters unlike any that have been built up to now because the initial beam size is large. The space in the ring lattice taken up by the injection/extraction system usually causes some problem because it changes the symmetry of the ring and displaces rf and absorbers, reducing cooling efficiency. The RC must be designed to accommodate the initial conditions of the muon beam when it is injected. As the beam gets cooled, all six dimensions shrink and the RC is less and less a good match to the beam size, especially from the standpoint of dispersion, absorber parameters, and rf frequency. Additional difficulties with ring coolers arise from the multiple passes of the beam through rf

cavities and absorbers, where rf beam loading and absorber heating issues are just being addressed.

Since the cooling channel that we are advocating in this paper is essentially a Linac filled with absorber, these difficulties are not issues. Injection and extraction, matching to the beam dimensions as the beam cools, and rf beam loading and absorber heating from multiple passes are not problems for a linear cooling channel.

RCs cannot easily take advantage of the pressurized high-gradient rf cavities being developed by Muons, Inc. and IIT at Fermilab. To use these rf cavities effectively, the entire ring would have to be filled with dense hydrogen gas since pressure windows would be counterproductive. Beam passing through areas without rf cavities would then suffer a large energy loss. Reducing the gas density could reduce the energy loss, but that would diminish the hoped-for gains of the pressurized cavities. Nevertheless, we note that the idea of using gas-filled ring coolers is being investigated with encouraging results [19].

RCs and the helical channel proposed here are similar in two respects. First, neither will easily accept a beam from a pion decay channel without some transverse precooling, rf bunching, and carefully matched injection parameters. Second, the helical channel has features of a weak focusing storage ring [20] (installed in a vertical plane, with an effective field index calculated below), where the orbits follow a spiral rather than a circular path.

II. GENERAL TECHNICAL APPROACH

A. Helical magnets

The technology of helical dipole magnets [21] is well known, for example at Brookhaven where helical “Siberian snakes” [22] are used for spin control in RHIC. A helical dipole can be

imagined as a superconducting dipole magnet wound on a beam tube, much like a Tevatron superconducting dipole, twisted about its axis so that the dipole bending field rotates its direction as the particle passes down the tube. A schematic of a helical dipole magnet [23] is shown in Figure 4. We note that for initial ionization cooling of a muon beam, the helical magnets may require four times the aperture than has been used up to now (~30 cm). Also note that the field of a helical dipole magnet is not intuitively obvious. For example, depending on the dimensions and period, the longitudinal and the transverse components can be comparable and have significant gradients. Given the right initial conditions, a particle will pass through this magnet on a helical trajectory about the magnet axis.

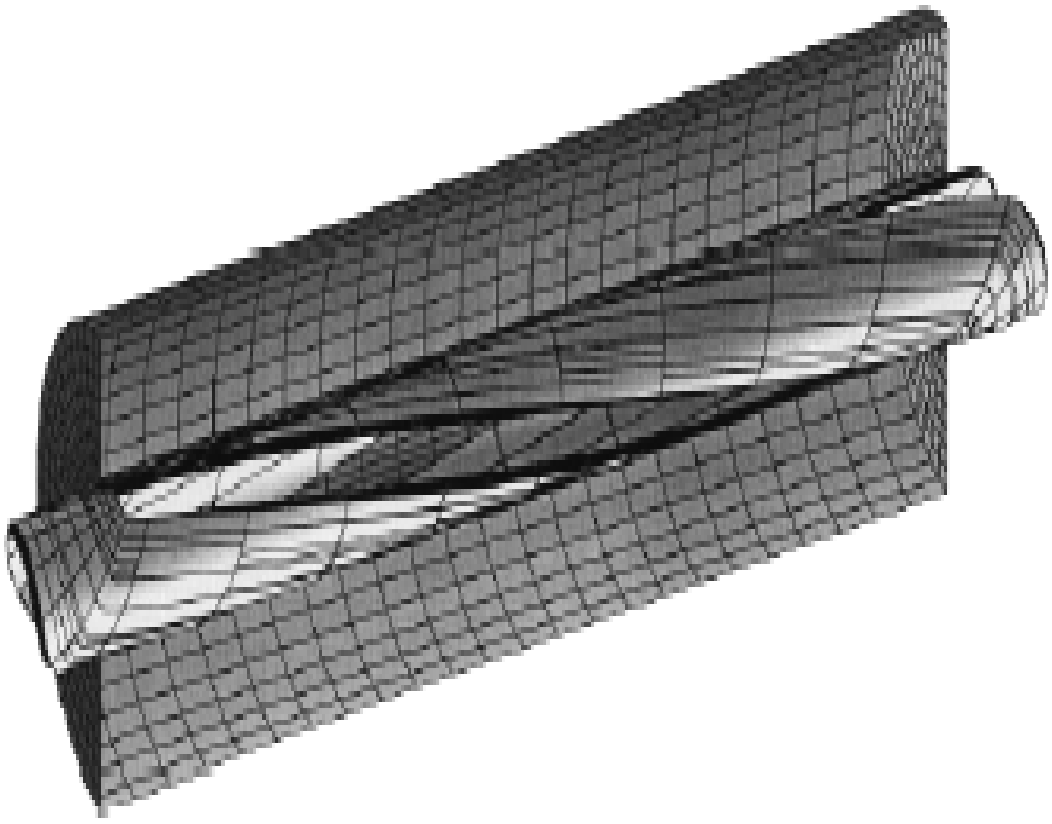

FIG. 4. Schematic representation of a helical dipole magnet showing the coil configuration and a cut-away view of the iron flux-return cylinder.

B. Helical cooling channel

The path of a muon traveling down a solenoid without helical magnets is also a helix, where the muon momentum transverse to the axis of the solenoid generates a projected circular orbit with the usual Larmor or cyclotron radius and frequency. If the muons pass through an energy absorber as is required for ionization cooling, the momentum and the cyclotron radius are reduced. This damping of transverse momentum in a solenoid without helical magnets is the basis for most schemes to accomplish transverse ionization cooling. Namely, rf cavities replace the energy lost in the absorber, boosting the beam momentum in the longitudinal direction so that the angular spread ($p_\perp / p_z$) is reduced until it is limited by multiple scattering in the absorber [24].

However, in order to cool the 6D emittance of a beam, the longitudinal motion must be moved to the transverse directions where ionization cooling is effective as indicated in figure 1b. This emittance exchange is accomplished in the channel proposed in this paper by superimposing a transverse helical dipole magnet to the solenoid on the same axis to make possible longitudinal as well as transverse cooling. As will be shown, the helical dipole magnet creates an outward radial force due to the longitudinal momentum of the particle while the solenoidal magnet creates an inward radial force due to the transverse momentum of the particle, or

$$\begin{aligned} F_{h-dipole} &\approx p_z \times B_\perp; \quad b \equiv B_\perp \\ F_{solenoid} &\approx -p_\perp \times B_z; \quad B \equiv B_z \end{aligned}, \tag{I.1}$$

where B is the field of the solenoid, the axis of which defines the z axis, and b is the field of the transverse helical dipole at the particle position. These are the Lorentz forces that are the starting point (III.6) for the derivations of the stability conditions for particle motion in these fields in section III. By moving to the rotating or helical frame of reference that follows the field of the helical dipole magnet, a time and z-independent Hamiltonian is then developed to explore the

characteristics of particle motion in the magnetic fields of the channel. After this, a continuous homogeneous energy absorber is added along with the "continuous" rf cavities needed to compensate for the energy loss and thus maintain the radius of the equilibrium orbit. Equations describing six-dimensional cooling in this channel are also derived, including explicit expressions for cooling decrements and equilibrium emittances.

Some of the actual theoretical development of this cooling channel was worked out some years ago by one of the authors [17]. In that work, the absorber was seen as composed of a homogeneous part and a part with a density gradient. Since the thinking at the time was that the wedge absorber scheme shown in Figure 1a should be dominant, especially in that discrete absorbers were always envisioned, the contributions from the homogeneous absorber were not considered as significant. The ideas and mathematical descriptions become more transparent in the case of a continuous homogeneous absorber. Much of the conceptual simplicity is lost in the case of discrete absorbers that must be carefully placed between magnetic coils and between rf cavities.

For a given beam momentum, one can vary the solenoid field and the strength and period of the helical dipole field. (The hydrogen gas energy-absorber density is also a free parameter provided the density is sufficient to suppress rf breakdown at the required level.) As we will demonstrate below, the helical field that must be superimposed on the solenoidal field must have a quadrupole component in addition to the dipole component in order to give the beam additional stability. This component could be added with "$\cos 2\theta$" quadrupole magnets having the same twist period as, and superimposed on, the helical dipole coils.

It is important to note that the direction of the solenoidal field does not change in the cooling channel described below. This is an essential difference between the helical dipole method and the solenoidal schemes with alternating field directions that have been envisioned up to now. This may also be some technical advantage to the extent that the large magnetic forces on the superconducting coils at the field reversal regions can be eliminated. Although a discussion of technical issues should follow the complete analysis of beam dynamics and cooling, we note that the use of continuous (or long) solenoids inherent in the helical concept should allow a higher maximum effective longitudinal field than that of schemes with alternating solenoidal field directions. Consequently, the helical scheme will achieve a smaller equilibrium emittance, faster cooling rate, and decreased particle loss from decay.

III. HELICAL ORBIT DYNAMICS

Beam dynamics in a helical channel has been studied for free electron lasers using a specific structure with only odd transverse field harmonics and a solenoid [25] and for a structure including a quadrupole harmonic but no solenoid [26]. Below we reproduce an analysis performed earlier [17] for the general case. In developing the cooling theory for a helical beam channel, the only important requirement is that the beam size $\sigma_\perp$ should be small with respect to the helix parameter. A small beam momentum spread is not assumed.

A. Notation

In this paper it is assumed that:

$-e = 1$, in order to simplify later equations involving magnetic fields;

$c = 1$;

$\vec{p}$ is the particle vector momentum;

$E = \gamma m = \sqrt{p^2 + m^2}$; $\beta = \sqrt{1 - \frac{1}{\gamma^2}}$;

$k = 2\pi/\lambda$, where λ is the transverse field period, and also the helical orbit period;

a is the helix orbit radius (a function of p);

$\kappa = ka$ is a in terms of $\lambda/2\pi$, such that $\kappa = p_\perp / p_z$ for the periodic orbit;

$D = p\frac{da}{dp}$ is the dispersion; $\hat{D} = D/a$ is the dispersion factor ;

x, y, z is the Cartesian laboratory frame;

$\vec{\rho} = (x, y)$ is the particle transverse coordinate relative to the structure axis;

ρ and φ are the axial coordinates:

$$x + iy = \rho e^{i\varphi};$$

$\hat{x}$ is the complex transverse coordinate in the rotating or helical frame:

$$\hat{x} = (x + iy)e^{-ikz} = \rho exp[i(\varphi - kz)];$$

$\vec{B} = \left(0, 0, B\right)$ is the solenoid field;

$k_c = B\sqrt{1 + \kappa^2}/p$;

$q = (k_c/k) - 1$;

b is the transverse magnetic field value at the periodic orbit;

$\vec{b}(x, y, z)$ is the 3-vector of the periodic field:

$$\vec{b}(x, y, z + \lambda) = \vec{b}(x, y, z).$$

The relationship between the helical magnetic field in the two frames is:

$$b_x + ib_y = (b_\rho + ib_\varphi)e^{i\varphi},$$

where b_ρ, b_φ, and b_z are functions of only ρ and $\psi \equiv \varphi - kz$;

Q_+ and Q_- are Q-values or tunes i.e. transverse oscillation frequencies about the periodic orbit;

ψ_+ and ψ_- are the phases of free transverse oscillations $(\psi'_\pm = kQ_\pm)$;

I_+ and I_- are the corresponding action variables (adiabatic invariants, or generalized Courant-Snyder invariants);

Λ_+ and Λ_- are the transverse cooling decrements $(I'_\pm = -\Lambda_\pm I_\pm$ after averaging over $\psi_\pm)$;

Λ_γ is the energy cooling decrement:

$$\Lambda_\gamma = -\frac{d}{d\gamma} < \gamma' >,$$

where the brackets $< ... >$ mean averaging over free transverse oscillations (i.e. $\psi_\pm$) and z.

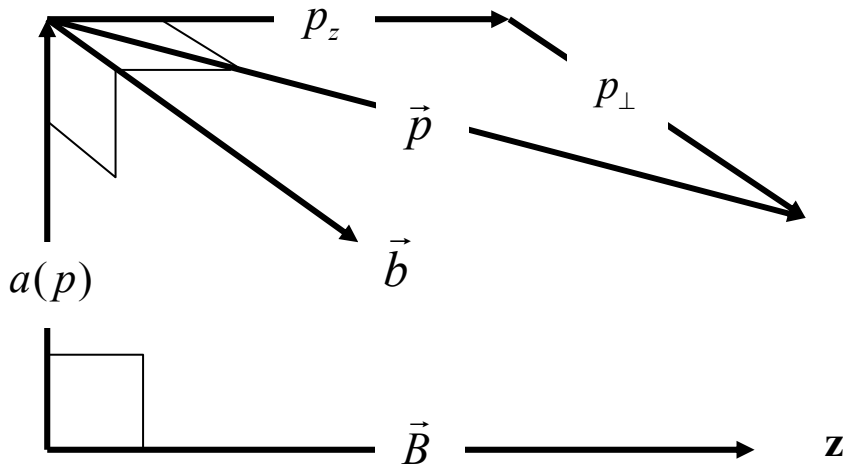

FIG. 5. Diagram of important relationships. The z axis coincides with the solenoid axis. At the periodic orbit, the transverse helical dipole field b is orthogonal to B and the radius vector a. The pitch angle of the helix is the arctan ($\kappa = p_\perp / p_z$).

Figure 5 shows some of the important geometrical relationships between the magnetic fields and particle coordinates used below. Consider a particle of momentum p at a radius of $a(p)$ in a stable helical orbit about the z axis of the structure, which is parallel to the solenoidal field B. The parameter $\kappa = p_\perp / p_z$ is the tangent of the pitch angle of the helical orbits. In the numerical example in chapter VI, this angle is 45 degrees and $\kappa = 1$ as shown in the figure. The transverse helical dipole field b is orthogonal to the z axis and to the radius vector a. The beam has to be specially prepared and injected into the channel so that the net transverse displacements and divergences of its centroid are matched to the helical equilibrium orbit.

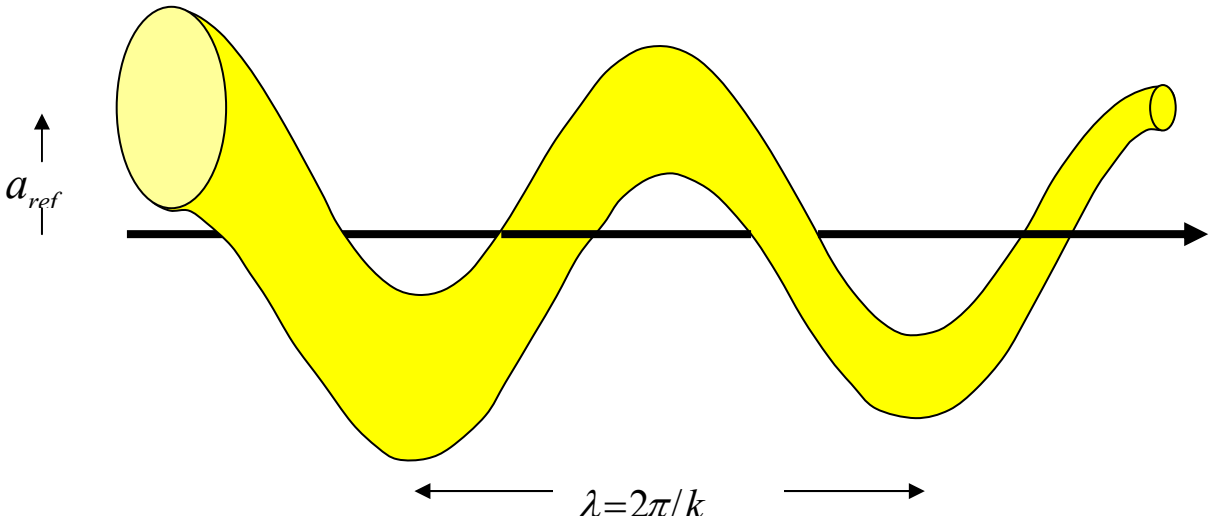

FIG 6. Illustration of motion of the beam envelope about the structure z-axis, which coincides with the solenoid center. The motion is in the gaseous hydrogen energy absorber that fills the volume of a contiguous series of pillbox rf cavities, which continuously replenish the lost energy. Superconducting coils outside the rf cavities provide the magnetic field of the helical channel.

Figure 6 is an illustration of how the beam envelope moves around the structure axis under the influence of the transverse dipole and solenoidal fields. The periodic equilibrium orbit is a helix of constant radius; particles oscillate transversely about this orbit and oscillate longitudinally with respect to the rf with frequencies or tunes as described below.

B. Helical field

A static magnetic field in vacuum can be represented as a gradient vector of a scalar function:

$$\vec{b} = \vec{\nabla} U,$$

where $U(\vec{r})$ satisfies the equation

$$\nabla^2 U = 0.$$

In the case of a helical structure, U should reflect helical invariance by being a function of $\psi \equiv \varphi - kz$ and ρ:

$$U(\vec{r}) = U(\rho, \psi).$$

Then

$$b_\rho = \frac{\partial U}{\partial \rho}, \quad b_\varphi = \frac{\partial U}{\rho \partial \varphi}, \quad \text{and} \quad b_z = -k\rho b_\varphi .$$

The Fourier expansion

$$U = \sum_{\ell \neq 0} U_\ell(\rho) e^{i\ell\psi}$$

leads to an equation for $U_\ell(\rho)$:

$$\frac{1}{\rho}\frac{d}{d\rho}\left(\rho \frac{dU_\ell}{d\rho}\right) - \left(\frac{1}{\rho^2} + k^2\right)\ell^2 U_\ell = 0 .$$

A solution regular at $\rho = 0$ is a modified Bessel function:

$$U_\ell = const \times I_\ell(\ell k\rho),$$

$$I_\ell(t) = \left(\frac{t}{2}\right)^\ell \sum_{n=0}^{\infty} \frac{(t^2/4)^n}{n!(n+\ell)!} \to \begin{cases} (\frac{t}{2})^\ell/\ell!, & t << 1 \\ \frac{e^t}{\sqrt{2\pi t}}, & t >> \ell^2 \end{cases} \quad \text{(III.1)}$$

Each harmonic is independent and corresponds to a current distribution

$$j_z, \quad j_\varphi \propto e^{i\ell\psi}$$

The most important harmonics are the dipole ($\ell = 1$),

$$\begin{aligned} b_\varphi &= 2b_d I_1(k\rho)(cos\psi)/k\rho \\ b_\rho &= 2b_d I_1'(k\rho) sin\psi \\ b_z &= -k\rho b_\varphi \end{aligned} \quad \text{(III.2)}$$

and quadrupole ($\ell = 2$):

$$\begin{aligned} b_\varphi &= (\frac{\partial b_\varphi}{\partial \rho})_o \frac{I_2(2k\rho)}{k^2\rho} cos2(\psi - \psi_2) \\ b_\rho &= \frac{1}{k}(\frac{\partial b_\varphi}{\partial \rho})_o I_2'(2k\rho) sin2(\psi - \psi_2) \\ b_z &= -k\rho b_\varphi, \qquad \psi_2 = const. \end{aligned} \quad \text{(III.3)}$$

where b_d and $(\frac{\partial b_\varphi}{\partial \rho})_o$ are the dipole and quadrupole strengths at $\rho = 0$, respectively. Sextupole ($\ell = 3$), and octupole ($\ell = 4$) harmonics might be needed for particular improvements. We note that this description corresponds to a field produced by simple external conductors and that other helical configurations of conductors are possible that would best be described by complementing the field description above with MacDonald functions. In fact, our considerations below rely only on the helical invariance of the fields and not on the details of the magnet design.

C. Equations of motion in a helical field

Here we derive the equations of motion in absence of absorbers and rf fields. Since the corresponding forces for absorbers and rf are weak, these effects can be treated using perturbative methods after the magnetic dynamical problem is solved. The Cartesian coordinates are the two transverse coordinates x, y, and the longitudinal coordinate z which coincides with the axis of the magnetic structure, having unit vectors $\vec{e}_x, \vec{e}_y, \vec{e}_z$. In the following calculations we use the definitions and relationships from above and

$$\frac{dz}{dt} \equiv (\dot{z}), \quad \beta_z dt = dz, \quad \frac{d}{dz} \equiv ('), \quad \vec{\rho} = (x, y), \tag{III.4}$$

$$\vec{p}_\perp = p_z \vec{\rho}', \quad \frac{p_z}{p} = \frac{\beta_z}{\beta} = \frac{1}{\sqrt{1+(\vec{\rho}')^2}}. \tag{III.5}$$

Let us use the initial Lorentz equation

$$\dot{\vec{p}} = (B\vec{e}_z + \vec{b}) \times \vec{\beta} \tag{III.6}$$

in order to into separate equations for transverse motion

$$\dot{\vec{p}}_\perp = (B + b_z)\vec{e}_z \times \vec{\beta}_\perp + \beta_z \vec{b}_\perp \times \vec{e}_z. \tag{III.7}$$

Using (III.4), (III.5) , and complex representation with

$$u = x + iy, \qquad i^2 = -1,$$

we can rewrite (III.7) as follows:

$$(p_z u')' = i(B + b_z)u' - i(b_x + ib_y). \tag{III.8}$$

This equation is complemented by the expression for p_z', which can easily be obtained using the conservation of total momentum, p,

$$p_z' = -\frac{1}{2} p \frac{(|u'|^2)'}{(1+|u'|^2)^{3/2}}. \tag{III.9}$$

Next, transform equation (III.8) to the rotating (helical) frame x_1, x_2, z with unit vectors $\vec{e}_1(z)$, $\vec{e}_2(z)$, $\vec{e}_z$, where the subscript 1 corresponds to the radial coordinate and field directions and the subscript 2 indicates the azimuthal coordinate and field directions.

Using the relationships

$$\hat{x} \equiv x_1 + ix_2 = ue^{-ikz} \ , \ u' = (\hat{x}' + ik\hat{x})e^{ikz} \ ,$$

$$\vec{\rho} = x\vec{e}_x + y\vec{e}_y = x_1\vec{e}_1 + x_2\vec{e}_2 \ ,$$

$$\vec{e}_x + i\vec{e}_y = (\vec{e}_1 + i\vec{e}_2)e^{ikz} \ , \text{ and}$$

$$b_x + ib_y = (b_1 + ib_2)e^{ikz} \ ,$$

we find

$$p_z(\hat{x}'' + 2ik\hat{x}' - k^2\hat{x}) + (p'_z - iB - ib_z)(\hat{x}' + ik\hat{x}) + i(b_1 + ib_2) = 0 \qquad \text{(III.10)}$$

with

$$p_z = \frac{p}{\sqrt{1+|\hat{x}' + ik\hat{x}|^2}}, \quad p'_z = -\frac{1}{2}p\frac{(|\hat{x}' + ik\hat{x}|^2)'}{(1+|\hat{x}' + ik\hat{x}|^2)^{3/2}} \ .$$

Recall that

$$b_z = k(x_2b_1 - x_1b_2),$$

and the transverse field components b_1 and b_2 are functions of only x_1 and x_2, but not z. Thus, the transverse x_1 and x_2 dynamics in the helical frame is conservative, although the equations are coupled and non-linear.

D. Helical orbits

1. Periodic orbits

It follows from the periodicity of the helical fields, that there will be periodic orbits with the same periodicity. The periodic orbit is determined as a solution of (III.10) at

$$\rho = const \equiv a, \quad x_1 = a, \quad x_2 = 0$$
$$\varphi' = const = k, \quad \text{i.e.}\, \psi' = 0, \quad \psi = 0$$
$$b_2 = b_2(ka) \equiv b, \quad b_1(\psi = 0) = 0$$
$$p_z = \frac{p}{\sqrt{1+\kappa^2}}.$$

The equilibrium equation is obtained as follows:

$$\frac{k_c}{k} - 1 = \frac{(1+\kappa^2)^{3/2}}{kp\kappa} b\,, \tag{III.11}$$

or

$$p(a) = \frac{\sqrt{1+\kappa^2}}{k}\left[B - \frac{1+\kappa^2}{\kappa} b \right], \tag{III.12}$$

or

$$\frac{b}{B} = \frac{\kappa}{1+\kappa^2}\left(1 - \frac{k}{k_c}\right) = \frac{\kappa}{1+\kappa^2}\left(\frac{q}{q+1}\right). \tag{III.13}$$

2. Dispersion

The dispersion factor

$$\hat{D} = \frac{p}{a}\frac{da}{dp}$$

plays a key role in the emittance exchange effect. It can be found immediately using the equilibrium equation (III.12):

$$\frac{p}{a}\frac{da}{dp} = \left(\frac{a}{p}\frac{dp}{da}\right)^{-1};$$

the result can be expressed as:

$$\hat{D}^{-1} = \frac{\kappa^2 + (1-\kappa^2)q}{1+\kappa^2} + g \tag{III.14}$$

where the effective field index at the periodic orbit is

$$g \equiv \frac{-(1+\kappa^2)^{3/2}}{pk^2}\frac{\partial b}{\partial a}. \tag{III.15}$$

Note, that the dispersion factor $\hat{D}$ does not vanish at $a \to 0$, while the dispersion $D = \hat{D}a$ disappears.

E. Transverse oscillations about the periodic orbit

1. Tunes of the helical orbits

Consider a position u_1, u_2 relative to the periodic orbit

$$u_1 = x_1 - a(p); \quad u_2 = x_2 \tag{III.16}$$

Assume $b_1 = 0$ and also $(\frac{\partial b_2}{\partial \psi}) = 0$ at $\psi = 0$. After a linear expansions of equation (III.10) with

$$k^2(u_1^2 + u_2^2) << 1, \quad (u_1')^2 + (u_2')^2 << 1, \tag{III.17}$$

and taking into account the field laws and equilibrium relationship in (III.11), we obtain two linear equations:

$$u_1'' + \frac{q-1}{1+\kappa^2}ku_2' + k^2\hat{D}^{-1}u_1 = 0, \tag{III.18}$$

and

$$u''_2 - (q-1)ku_1' + k^2(q-g)u_2 = 0. \tag{III.19}$$

These equations are conservative but coupled. The coupling is due to a difference between the Coriolis force and the non-equilibrium part of the Lorentz force of the solenoid. At

$k_c = 2k$, u_1 and u_2 become decoupled (in linear approximation). In the following development we do not assume that u_1 and u_2 are decoupled, but treat the general case. The solution of these equations can be found as eigenvectors

$$\begin{pmatrix} u_1 \\ u_2 \end{pmatrix} = \begin{pmatrix} c_1 \\ c_2 \end{pmatrix} e^{ikQz}, \quad \text{at} \quad \begin{pmatrix} c_1 \\ c_2 \end{pmatrix} = const,$$

where we obtain the zero determinant equation:

$$Q^4 - 2Q^2 R + G = 0, \tag{III.20}$$

with

$$G \equiv \left(q - g\right)\hat{D}^{-1} = \left(\frac{2q + \kappa^2}{1 + \kappa^2} - \hat{D}^{-1}\right)\hat{D}^{-1} \tag{III.21}$$

and

$$R \equiv \frac{1}{2}\left(1 + \frac{q^2}{1 + \kappa^2}\right). \tag{III.22}$$

Thus, the Q-values are found:

$$Q^2 = Q_{\pm}^2 \equiv R \pm \sqrt{R^2 - G}, \tag{III.23}$$

and the stability area is established:

$$0 < G < R^2. \tag{III.24}$$

Note that

$$Q_+^2 \cdot Q_-^2 = G, \tag{III.25}$$

while

$$Q_+^2 + Q_-^2 = 2R. \tag{III.26}$$

Thus we have two tunes for the normal mode oscillations. For a solenoidal field alone, there is only a single frequency, but when the helical field is added the frequency is split.

2. Transverse oscillations

Using equation (III.18), we find the normal oscillation behavior:

$$X_{\pm} \equiv \begin{vmatrix} u_1 \\ u'_1 \\ u_2 \\ u'_2 \end{vmatrix}_{\pm} = a_{\pm} \begin{vmatrix} cos\psi_{\pm} \\ -kQ_{\pm} sin\psi_{\pm} \\ (\alpha_{\pm}/Q_{\pm}) sin\psi_{\pm} \\ k\alpha_{\pm} cos\psi_{\pm} \end{vmatrix}, \tag{III.27}$$

where $a_{\pm} = const$, $\psi_{\pm} = Q_{\pm} kz + const$, and

$$\alpha_{\pm} = \frac{1+\kappa^2}{q-1}(Q_{\pm}^2 - \hat{D}^{-1}) .$$

We note the useful relationships:

$$\hat{D}\alpha_{+}\alpha_{-} = -(1+\kappa^2) \tag{III.28}$$

and

$$\frac{Q_{+}^2}{\alpha_{+}} - \frac{Q_{-}^2}{\alpha_{-}} = \frac{\alpha_{+} - \alpha_{-}}{1+\kappa^2} = \frac{2}{q-1}\sqrt{R^2 - G} . \tag{III.29}$$

The general solution X is a sum of $X_{\pm}$ and the helix path:

$$\begin{vmatrix} x_1 \\ x'_1 \\ x_2 \\ x'_2 \end{vmatrix} = X_{+} + X_{-} + \begin{vmatrix} a(p) \\ 0 \\ 0 \\ 0 \end{vmatrix} . \tag{III.30}$$

3. Amplitudes

The solution in (III.27) can be treated also as a transformation from x_1, x'_1, x_2, x'_2 to variables of amplitudes and phases of normal mode oscillations. This is reasonable to the extent

that perturbative forces related to non-linearities or non-adiabatic changes of fields and absorbers are small during a single oscillation period. The squared amplitudes are of primary importance. The transformed relationships can be easily found using (III.27) and (III.30):

$$x_2' - k\alpha_{\mp}(x_1 - a) = (\alpha_{\pm} - \alpha_{\mp})ka_{\pm}cos\,\psi_{\pm}, \tag{III.31}$$

and

$$\alpha_{\mp}x_1' + kQ_{\mp}^2 x_2 = \frac{1}{Q_{\pm}}(\alpha_{\pm}Q_{\mp}^2 - \alpha_{\mp}Q_{\pm}^2)ka_{\pm}sin\,\psi_{\pm}. \tag{III.32}$$

Thus,

$$k^2 a_+^2 = \frac{[x_2' - \alpha_- k(x_1 - a)]^2}{(\alpha_+ - \alpha_-)^2} + Q_+^2 \frac{(\alpha_- x_1' + Q_-^2 kx_2)^2}{(\alpha_+ Q_-^2 - \alpha_- Q_+^2)^2} \tag{III.33}$$

and

$$k^2 a_-^2 = \frac{[x_2' - \alpha_+ k(x_1 - a)]^2}{(\alpha_+ - \alpha_-)^2} + Q_-^2 \frac{(\alpha_+ x_1' + Q_+^2 kx_2)^2}{(\alpha_+ Q_-^2 - \alpha_- Q_+^2)^2}. \tag{III.34}$$

4. Transverse adiabatic invariants

The effective beam volume in phase space is measured in terms of action variables, or adiabatic invariants $I_{\pm}$, canonically conjugate with the oscillation phases $\psi_{\pm}$. They are proportional to squared amplitudes:

$$I_{\pm} = \frac{1}{2}\beta\gamma k Q_{\pm} a_{\pm}^2 \cdot R_{\pm}, \tag{III.35}$$

where we have introduced the coefficients $R_{\pm}(E)$. To find them, one can use the canonical relationships (see the Appendix):

$$\frac{\partial}{\partial E} I_{\pm}(\vec{P}_{\perp}, \vec{\rho}, E) = -\frac{\partial}{\partial \psi_{\pm}} t(I_{\pm}, \psi_{\pm}), \tag{III.36}$$

where the energy $(-E)$ and time (t) are considered as one of three "old" canonical pairs, together with $\vec{p}_\perp$ and $\vec{\rho}$ (while the z coordinate is treated as the "time argument"). To determine the time t as function of "new" variables $(a_\pm, \psi_\pm)$, one has to integrate the equation

$$t' = \frac{1}{\beta_z}$$

along a "solved" particle trajectory. In linear approximation for free particle oscillations near the helical orbit $\vec{a}(p,z)$ we have (see the Appendix)

$$t = \hat{t} + \frac{\kappa}{\beta\sqrt{1+\kappa^2}}\left[\frac{1+\alpha_+}{Q_+}a_+ sin\psi_+ + \frac{1+\alpha_-}{Q_-}a_- sin\psi_-\right],\ \hat{t}' = const., \tag{III.37}$$

where we have introduced a "shortened time" $\hat{t}$ as a new canonical variable conjugate to the energy, -E. Using the relationships (III.32) and (III.37), the shortened time can be expressed as a function of initial variables:

$$\hat{t} = t + \frac{1}{\beta\sqrt{1+\kappa^2}}\left[Dx_1' + \left(1 - \frac{q-1}{1+\kappa^2}\hat{D}\right)\kappa x_2\right]. \tag{III.38}$$

Note that the rate $\hat{t}$ changes is constant on a particle trajectory in a magnetic field.

Returning to the derivatives $\frac{\partial a_\pm^2}{\partial E}$, they can be found using the relationships in (III.35) through (III.37), in which the variables of the rotating frame (x_1, x_1', x_2, x_2') are to be considered as functions of $(x, p_x), (y, p_y)$, and energy E. The calculation in the Appendix gives

$$\frac{\partial}{\partial E}a_\pm^2 = \mp\frac{2a(1+\kappa^2)}{E\beta^2}\frac{1+\alpha_\pm}{\alpha_\pm}a_\pm cos\psi_\pm. \tag{III.39}$$

Using equations (III.35), (III.36), and (III.37) gives

$$R_\pm = \pm\frac{\alpha_\pm}{(1+\kappa^2)^{3/2}}\cdot\frac{\alpha_+ - \alpha_-}{Q_\pm^2}. \tag{III.40}$$

Thus solutions and relationships (III.31) through (III.40) provide a full set of canonical transformations from the initial variables $(\vec{p},\vec{r})$ to action and phase variables in a magnetic field before an rf field has been introduced.

5. Beam envelopes on a helical orbit

In the rotating frame of the helical orbit, each of the two normal mode oscillations is recognized in transverse space as an elliptical orbit with tune Q_+ or Q_- (see equation (III.27):

$$\left|\begin{matrix}u_1\\u_2\end{matrix}\right|_+ = a_+\left|\begin{matrix}\cos\psi_+\\(\alpha_+/Q_+)\sin\psi_+\end{matrix}\right|,\quad \left|\begin{matrix}u_1\\u_2\end{matrix}\right|_- = a_-\left|\begin{matrix}\cos\psi_-\\(\alpha_-/Q_-)\sin\psi_-\end{matrix}\right|. \tag{III.41}$$

With random phase distributions, there are two normal beam ellipsoids of aspect ratios

$$\left(\frac{\sigma_1}{\sigma_2}\right)_+ = \frac{Q_+}{\alpha_+},\quad \left(\frac{\sigma_1}{\sigma_2}\right)_- = \frac{Q_-}{\alpha_-}. \tag{III.42}$$

For ensembles with adiabatic invariants $I_\pm$, one can average over $\psi_\pm$ to find the related sizes σ_1 and σ_2:

$$(\sigma_1)_\pm^2 = \pm\frac{I_\pm Q_\pm}{\gamma\beta k\alpha_\pm(\alpha_+-\alpha_-)},\quad (\sigma_2)_\pm^2 = (\sigma_1)_\pm^2\left(\frac{\alpha_\pm}{Q_\pm}\right)^2. \tag{III.43}$$

Thus, σ_1 and σ_2 rms sizes can be explicitly found as determined by the two canonical (and uncorrelated) emittances ε_+ and ε_- by substituting for $I_\pm$ with $\langle I_\pm\rangle = \varepsilon_\pm$ into (III.43) and adding a contribution due to energy spread:

$$\sigma_1^2 = D^2\left(\frac{\Delta p}{p}\right)^2 + (\sigma_1)_+^2 + (\sigma_1)_-^2,\quad \sigma_2^2 = (\sigma_2)_+^2 + (\sigma_2)_-^2 \tag{III.44}$$

The canonical emittances, $\varepsilon_\pm$, will not be disturbed by an adiabatic change of beam optics parameters along the beam path in the helical transport line. These uncorrelated emittances (i.e.

the averaged values of adiabatic or generalized Courant-Snyder invariants) also can be conserved in transfers from the helical channel to sections with different optics, such as a conventional alternating gradient transport with uncoupled planes. However, special optics will be needed to match such a transition in order to avoid an increase of beam emittances.

F. Longitudinal oscillations in an rf field

An rf field has to be applied to compensate for energy loss in an absorber to achieve substantial ionization cooling. Thus the beam must first be captured and bunched before the cooling described in this paper can be accomplished. The capture and bunching processes will be described in a paper to follow this one. In this section we introduce the basic characteristics of longitudinal dynamics of particles in a bunched beam subject to an rf field on a helical beam path without absorber.

1. Basic equations

Longitudinal motion of particles in an rf field is governed by equations for energy E and time t as a pair of canonically conjugate variables, with the z coordinate considered a time argument and the rf wave number k_{rf} expressed in terms of the rf cavity resonant frequency and particle longitudinal velocity,

$$k_{rf} \approx \omega / \beta_z .$$

Assuming, as usual, that the change of particle energy along one period of magnetic and electric field and "betatron" oscillations is small, we can express the equations in terms of energy and shortened or average time t, given by equations (III.37) and (III.38). A convenient variable is a reference time

$$\tau = \hat{t} - \left(k_{rf} / \omega \right) z . \qquad \text{(III.45)}$$

Note that the rate of change of $\hat{t}$ as a function of z is not influenced by particle transverse oscillations in a focusing magnetic field. Neglecting the phase $\omega\tau$ and the rate of change of energy on transverse amplitudes, we obtain the shortened canonical equations:

$$\gamma' = -\gamma'_{\max} \sin\omega\tau = -\frac{\partial}{\partial\tau} H_S \text{ and} \tag{III.46}$$

$$\tau' = \frac{1}{\beta}\sqrt{1+\kappa^2} - \frac{k_{rf}}{\omega} = \frac{\partial}{\partial\gamma} H_S , \tag{III.47}$$

where

$$H_S = \int\left(\frac{1}{\beta}\sqrt{1+\kappa^2} - \frac{k_{rf}}{\omega}\right)d\gamma - \frac{\gamma'_{\max}}{\omega}\cos\omega\tau \tag{III.48}$$

is the effective longitudinal or synchrotron Hamiltonian, and $\gamma'_{\max}$ is the maximum rate of energy change due to the rf field.

The Hamiltonian and equations (III.46) and (III.47) determine the equilibrium phase $\omega\tau = 0$, the equilibrium or resonance energy γ_{res} such that

$$\left(\frac{1}{\beta}\sqrt{1+\kappa^2}\right)_{\gamma=\gamma_{res}} = \frac{k_{rf}}{\omega} , \tag{III.49}$$

and the phase space trajectory of particle oscillations around the equilibrium orbit where

$$H_S(\gamma,\tau) = const. \tag{III.50}$$

2. Translational mobility of a particle on a helical path

For a particle of energy $E = m\gamma$, the rate of change of phase is given in linear approximation by

$$\hat{\tau}' = \eta(\gamma - \gamma_{res}) \equiv \eta\,\Delta\gamma \tag{III.51}$$

where we have introduced a new parameter, η, the translational mobility:

$$\eta = \frac{d}{d\gamma}\frac{\sqrt{1+\kappa^2}}{\beta} = \frac{\sqrt{1+\kappa^2}}{\gamma\beta^3}\left(\frac{\kappa^2}{1+\kappa^2}\hat{D} - \frac{1}{\gamma^2}\right). \tag{III.52}$$

This parameter is analogous to the momentum slip factor in a synchrotron, where the factor $\frac{\kappa^2}{1+\kappa^2}\hat{D}$ can be identified with $\frac{1}{\gamma_{transition}^2}$.

3. Synchrotron tune

The rate of change of energy for a particle with phase $\omega\tau$ is given in linear approximation by

$$\Delta\gamma' = -\gamma'_{\max}\,\omega\tau\,. \tag{III.53}$$

Equations (III.51) and (III.53) determine the synchrotron tune, the frequency of phase and energy oscillations near the equilibrium where $\tau = 0$ and $\gamma = \gamma_{res}$:

$$\tau'' + \omega^2 Q_S^2 \tau = 0\,, \text{ and } Q_S^2 = \eta\gamma'_{\max}/\omega\,. \tag{III.54}$$

4. Synchrotron adiabatic invariant, canonical phase, and admittance

The adiabatic invariant of oscillations about the equilibrium is determined as an area in phase space bounded by the ellipse given by equation (III.50):

$$I_S = \frac{1}{2\pi}\oint \Delta\gamma\, d\tau\,. \tag{III.55}$$

For a small oscillation near the equilibrium, I_S is proportional to the Hamiltonian function:

$$I_S \approx \frac{H_S}{\omega Q_S} = \frac{\eta}{2\omega Q_S}\left(\Delta\gamma\right)^2 + \frac{\omega Q_S}{2\eta}\tau^2\,. \tag{III.56}$$

More generally, there is the relationship

$$dH_S = \omega Q_S\left(I_S\right) dI_S$$

with $Q_S\left(I_S\right)$ as the amplitude-dependent synchrotron frequency that takes into account the non-linear behavior of the rf field as a function of phase $\omega\tau$. A canonical variable conjugate to the synchrotron invariant I_S is the synchrotron phase Ψ_S, which varies uniformly on an unperturbed orbit:

$$\Psi'_S = \omega Q_S\left(I_S\right). \tag{III.57}$$

The maximum I_S value for captured particles, the admittance, corresponds to oscillations near the synchrotron separatrix:

$$H_S = \frac{\gamma'_{\max}}{\omega}, \text{ and } \left(I_S\right)_{adm} = \frac{2}{\pi\omega}\sqrt{\frac{\gamma'_{\max}}{\eta\omega}} \tag{III.58}$$

On the separatrix trajectory, the frequency Q_S is zero due to the points $\omega\tau = \pm\pi$.

IV. COOLING DECREMENTS

A. Absorber drag force

Muons passing through an absorber experience energy and momentum loss due to collisions with electrons. The collision effect averaged over impact parameters is described by the well-known formula for the drag force:

$$\dot{\vec{p}} = \frac{-F\,\vec{p}}{p}, \quad F = \frac{4\pi Z n e^4 \log}{m_e \beta^2}, \tag{IV.1}$$

where Z and n are the absorber atomic number and concentration, m_e the electron mass, and β is the muon velocity. Here log is a symbol for the Coulomb logarithm of ionization energy loss for fast particles:

$$\log \equiv \ln\left(\frac{2p^2}{h\nu m_\mu}\right) - \beta^2, \tag{IV.2}$$

with $h\nu$ the effective ionization potential [27]. A typical magnitude of the log is about 12 for the conditions described below.

Similar to the radiation force for relativistic electrons in a magnetic field, the drag force produces a damping effect on muon transverse oscillations in a focusing field:

$$\vec{p}'_\perp = -\Lambda_0 \vec{p}_\perp, \quad \Lambda_0 = \frac{F}{\gamma\beta^2 m_\mu}.$$

Unlike the radiation force, however, the drag force cannot damp the beam energy spread since its characteristic energy dependence, dF/dE, is negative or is too small when it is positive ($\gamma^2 > \log$):

$$E' = -F(E), \quad \Delta E' = -\left(dF/dE\right)\Delta E,$$

$$\left(dF/dE\right) = 2\Lambda_0\left[-\frac{1}{\gamma^2} + \frac{1-\left(\beta/\gamma\right)^2}{\log}\right]. \tag{IV.3}$$

To achieve longitudinal cooling requires emittance exchange with transverse oscillations as discussed in Section II. Emittance exchange, in turn, requires the introduction of a beam bend that creates dispersion, a correlation between the orbit and energy of a particle. Use of a continuous homogeneous absorber, rather than wedges at discrete points, implies a positive dispersion along the entire cooling path, a condition that we have shown exists for an appropriately designed helical dipole channel. We have also shown that this condition is compatible with stable periodic orbits.

The linear theory of the damping process including wedge effects was developed earlier [15] and later applied and developed in some detail for a homogenous absorber [17]. The treatment in this paper follows the analysis in these previous works but includes more detail.

Below we will calculate the longitudinal and transverse damping rates along a helical transport line in a homogeneous absorber with rf fields. As an example of how the cooling rates can be manipulated, we will then indicate how to achieve balanced 6D cooling, where the three decrements are equal.

B. Longitudinal decrement

1. Synchrotron oscillations in the absorber

Energy loss due to muon collisions with absorber electrons can be included after averaging over collision parameters and transverse oscillations about the energy-dependent helical orbit:

$$\gamma' = -\gamma'_{\max} \sin \omega\tau - \frac{F}{m_\mu}\sqrt{1+\kappa^2}\ . \tag{IV.4}$$

Expanding energy loss in a linear approximation as a function of energy near the reference orbit, we obtain synchrotron oscillation equations:

$$\Delta\gamma' = -\gamma' \left(\sin \omega\tau - \sin \omega\tau_{eq}\right) - \Lambda_\gamma \Delta\gamma\,, \tag{IV.5}$$

where

$$\gamma'_{\max} \sin \omega\tau_{eq} = -\frac{F}{m_\mu}\sqrt{1+\kappa^2}\Bigg|_{\gamma=\gamma_{res}} \tag{IV.6}$$

and we have introduced the energy decrement as

$$\Lambda_\gamma = \frac{d}{d\gamma}\frac{<F>}{m_\mu}\sqrt{1+\kappa^2} = \left[-\frac{2}{\gamma^2} + \frac{2\left(1-\left(\beta/\gamma\right)^2\right)}{\log} + \hat{D}\frac{\kappa^2}{1+\kappa^2}\right]\Lambda_0\,. \tag{IV.7}$$

For positive Λ_γ, synchrotron oscillations will damp with a characteristic exponent Λ_γ. Note that the synchrotron oscillations in the absorber may last some time since

$$\Lambda_\gamma \ll \omega Q_S\,, \tag{IV.8}$$

where $Q_s^2 = \eta\omega\gamma'_{\max}\cos\omega\tau_{eq}$.

The relationship (IV.8) follows from the condition $\gamma' \ll \omega\gamma_{res}$, taking into account that $\Lambda \sim \gamma'_{\max}/\gamma_{res}$ unless the translational mobility parameter η is very small. Consequently we can continue to treat the phase $\omega\tau$ and energy motion in terms of oscillations even though the reduction in the synchrotron potential well might not be small ($F \le m\gamma'$). We can characterize the oscillations by a modified synchrotron adiabatic invariant as determined by the integral in (III.55), but with a Hamiltonian

$$\hat{H} = \frac{\eta}{2}(\Delta\gamma)^2 - \gamma'_{\max}\left(\cos\omega\tau + \omega\tau\sin\omega\tau_{eq}\right)/\omega\,. \tag{IV.9}$$

Damping due to an emittance exchange mechanism can then be considered a slow process.

2. Synchrotron oscillation decrement

Under condition (IV.8) one can calculate the damping rate of I_S using a perturbative method. Considering the adiabatic invariant a function of $\Delta\gamma$ and $\omega\tau$ we find the instantaneous and average rates of change of the adiabatic invariant:

$$I_S{}' = -\frac{\partial I_S}{\partial\gamma}\Lambda_\gamma\,\Delta\gamma\,.$$

Using the canonical relationship $\dfrac{\partial I_S}{\partial\gamma} = \dfrac{\partial\tau}{\partial\Psi_S}$ and taking into account that

$$\tau' = \frac{\partial\tau}{\partial\Psi_S}\Psi'_S = \frac{\partial\tau}{\partial\Psi_S}\omega Q_S\left(I_S\right),$$

we find a simple damping equation:

$$< I_S' >= -\Lambda_\gamma \oint \Delta\gamma \, d\tau / 2\pi = -\Lambda_\gamma I_S \,. \tag{IV.10}$$

Note that the linear reduction of the Hamiltonian has not been used in this derivation. Thus in the approximation of a constant energy decrement as in (IV.5), the non-linearity of synchrotron oscillations does not affect the cooling rate.

Note, finally, that the instantaneous rate of change of phase $\omega\,\tau$ is influenced by the transverse component of the drag force ($\sim x_1'$) according to equation (III.38), but the average effect is zero:

$$< \tau \, \delta\tau' > \sim < \tau \frac{\partial \hat{t}}{\partial x_1'} x_1' >= 0 \,.$$

C. Transverse decrements

To derive the transverse rates, we have to calculate the average partial power $< I_\pm' >$. This can be easily done considering $I_\pm$ as functions of transverse vector momentum $\vec{p}_\perp$, coordinate $\vec{\rho}$, and energy $E = m\gamma$:

$$I_\pm' = \frac{1}{\beta_z} \frac{\partial I_\pm}{\partial \vec{p}_\perp} \vec{F}_\perp + \frac{\partial I_\pm}{\partial \gamma} \cdot \gamma' \,, \tag{IV.11}$$

with

$$\vec{F}_\perp = -F \cdot \frac{\vec{\beta}_\perp}{\beta} = -F \frac{\vec{\rho}' \beta_z}{\beta}, \quad \gamma' = -\frac{F}{m_\mu} \sqrt{1 + (\vec{\rho}')^2} \,. \tag{IV.12}$$

We avoid the derivation of the expressions $I_\pm(\vec{p}_\perp, E, \vec{\rho}, z)$; instead, we use the canonical relationships shown in the Appendix, (IX.6) and (IX.7), then

$$I_\pm' = -F \left[\frac{1}{\beta} \vec{\rho}' \frac{\partial \vec{\rho}}{\partial \psi_\pm} - \frac{\partial t}{\partial \psi_\pm} \sqrt{1 + (\vec{\rho}')^2} \right]. \tag{IV.13}$$

Thus, we can simply use the solutions in (III.27) and (III.37) in order to perform averaging over the phases $\psi_{\pm}$. Note that

$$\vec{\rho}' \frac{\partial \vec{\rho}}{\partial \psi_{\pm}} = Re(\hat{x}' \frac{\partial \hat{x}^*}{\partial \psi_{\pm}}) \text{ and}$$

$$\sqrt{1+(\vec{\rho}')^2} \approx \sqrt{1+\kappa^2} + \frac{\kappa}{\sqrt{1+\kappa^2}}(ku_1 + u_2'). \tag{IV.14}$$

The force F has to be taken as shown in (IV.12). The right parts of equations (IV.11) after averaging over $\psi_{\pm}$ become proportional to $a_{\pm}^2$ (see (III.27)), i.e. the cooling decrements can be defined:

$$< I'_{\pm} >= -\Lambda_{\pm} I_{\pm},$$

taking into account (III.35). Performing the averaging, we find:

$$\frac{\Lambda_{\pm}}{\Lambda_o} = \pm \frac{1+\kappa^2}{(\alpha_+ - \alpha_-)\alpha_{\pm}} \left[2\alpha_{\pm} + \alpha_{\pm}^2 + Q_{\pm}^2 - \frac{\kappa^2}{1+\kappa^2}(1+\alpha_{\pm})^2 \right]. \tag{IV.15}$$

Taking into account relationships in (III.28) and (III.29), we find the sum of transverse decrements:

$$\frac{\Lambda_+ + \Lambda_-}{\Lambda_o} = 2 - \frac{\kappa^2}{1+\kappa^2}\hat{D}. \tag{IV.16}$$

Combining all the three decrements, we find:

$$\Lambda_+ + \Lambda_- + \Lambda_\gamma = 2\Lambda_o \cdot \left(\beta^2 + \frac{1}{2}\frac{p}{log}\frac{\partial log}{\partial p} \right) \equiv \Lambda = 2\Lambda_0 \hat{\beta}^2, \tag{IV.17}$$

where we have introduced the parameter

$$\hat{\beta} = \sqrt{\beta^2 + \frac{1}{2}\frac{p}{\log}\frac{\partial \log}{\partial p}} = \sqrt{\beta^2 + \frac{1-(\beta/\gamma)^2}{\log}}, \tag{IV.18}$$

although in the following we will not distinguish between $\hat{\beta}$ and β, assuming

$$\beta^2 \gg \frac{1}{2}\frac{p}{log}\frac{\partial log}{\partial p}.$$

This result (IV.17) agrees with the dissipation theorem [28,29,30]:

$$\sum_{\alpha=1}^{3}\Lambda_\alpha = -<\frac{1}{\beta_z}\frac{\partial}{\partial \vec{p}}\vec{F}(\vec{p},\vec{r})>.$$

The distribution of the two transverse cooling rates is characterized by the difference $\Lambda_+ - \Lambda_-$. Using the definitions $\alpha_\pm$, etc., we obtain:

$$\frac{\Lambda_+ - \Lambda_-}{\Lambda_o} = \frac{1}{\sqrt{R^2 - G}}\left[q^2 - 1 + \kappa^2(R\hat{D} - 1)\right]\frac{1}{1+\kappa^2}. \qquad \text{(IV.19)}$$

D. Equating the cooling decrements

If the three cooling decrements are equal,

$$\Lambda_\gamma = \Lambda_+ = \Lambda_- = \Lambda/3,$$

then

$$\hat{D} = 2\frac{1+\kappa^2}{\kappa^2}\left(1 - \frac{2}{3}\beta^2\right) \qquad \text{(IV.20)}$$

and

$$q \equiv \frac{k_c}{k} - 1 = \beta\sqrt{\frac{1+\kappa^2}{3-\beta^2}}. \qquad \text{(IV.21)}$$

As follows from formula (III.14), conditions (IV.20) and (IV.21) also determine the effective field index g as a function of κ and β:

$$g = -\frac{1-\kappa^2}{1+\kappa^2}\beta\sqrt{\frac{1+\kappa^2}{3-\beta^2}} + \frac{\kappa^2}{2(1+\kappa^2)}\frac{4\beta^2 - 3}{3 - 2\beta^2}. \qquad \text{(IV.22)}$$

Condition (IV.21) indicates the necessity of sufficiently strong solenoidal and dipole fields according to equations (III.11) or (III.13), while condition (IV.22) determines the quadrupole strength.

The balanced cooling area in terms of parameters κ and β can be limited by the dynamical stability condition (III.24), which can be rewritten as

$$0 < \left(\beta \left(\frac{1+\kappa^2}{3-\beta^2} \right)^{1/2} + \kappa^2 \frac{\frac{3}{4}-\beta^2}{3-2\beta^2} \right) < \left(\frac{(1+\kappa^2)^2}{4\kappa^2} \frac{(1-\frac{2}{3}\beta^2)}{(1-\frac{1}{3}\beta^2)^2} \right). \quad \text{(IV.23)}$$

In the region $\beta^2 < 3/4$, the periodic orbit seems to appear stable at any κ value, although for $\beta^2 > 3/4$ condition (IV.21) also leaves the beam stable in a wide range of $\kappa < 1$. Note, however, that if κ is too small then the beam stability is worse, as can be seen from the formula for the oscillation tune Q_-;

$$Q_- \approx \sqrt{G/2R} \approx \kappa \left(\frac{\sqrt{3-\beta^2}}{3-2\beta^2} \beta \right)^{1/2}. \quad \text{(IV.24)}$$

V. EQUILIBRIUM EMITTANCES

A. Scattering and straggling

Besides the average ionization energy loss when moving through the absorber, each muon exchanges momentum with the atoms of the absorber, both in direction and magnitude. The average angular scattering from absorber nuclei and electrons is:

$$\frac{d\theta_{sc}^2}{dz} = \frac{Z+1}{\gamma\beta^2} \frac{m_e}{m_\mu} \Lambda. \quad \text{(V.1)}$$

The spread about the average energy loss is effectively only caused by collisions with electrons, because of the large nucleon mass relative to the electron mass:

$$\frac{d}{dz}\left(\delta\gamma\right)^2 = \frac{\gamma\beta^2}{4log}\left(\gamma^2+1\right)\frac{m_e}{m_\mu}\Lambda\,. \tag{V.2}$$

It is well known that the momentum or energy spread does not include the factor of the Coulomb log since it is determined characteristically by interactions with the maximum momentum transfer. The contribution of low momentum transfer collisions to energy diffusion appears insignificant, contributing at most to angular scattering and energy loss. Correspondingly, the energy straggling grows rapidly with the Lorentz factor of the muon beam.

B. Longitudinal equilibrium emittance, energy spread, and bunch length

The equilibrium synchrotron emittance results from the balance between damping and growth rates due to both energy straggling and angle scattering. In the vicinity of the reference orbit, the adiabatic invariant can be represented as a quadratic function of energy deviation from the equilibrium value and reference time τ as shown in (III.56). Then the diffusion growth rate of I_S can generally be found as

$$\left(I_S{}'\right)_d = \frac{\eta}{2\omega Q_S}\frac{d}{dz}\left(\delta\gamma\right)^2 + \frac{\omega Q_S}{2\eta}\frac{d}{dz}\left(\delta\hat{t}\right)^2, \tag{V.3}$$

where the straggling rate is given by formula (V.2). The diffusion rate of $\hat{t}$ can be found using equation (III.38) taking into account the continuity of the total phase, $\omega t - k_{rf} z$, in a collision,

$$\frac{d}{dz}\left(\delta\hat{t}\right)_{sc}^2 = \frac{D^2}{2\beta^2\left(1+\kappa^2\right)}\frac{d}{dz}\theta_{sc}^2 \tag{V.4}$$

with the angle scattering rate as given by (V.1).

Applying the Langevin balance equation [31]:

$$I_S' = -\Lambda_\gamma I_S + \left(I_S'\right)_d,$$

we obtain the normalized equilibrium synchrotron emittance:

$$\varepsilon_S \equiv < I_S >_{eq} = \left(I_S'\right)_d / \Lambda_\gamma = \frac{\Lambda}{4\Lambda_\gamma}\frac{m_e}{m_\mu}\gamma\beta^2\left[\frac{\eta}{\omega Q_S}\frac{\gamma^2+1}{2\log} + \frac{Z+1}{\gamma^2\beta^6}\frac{\omega Q_S}{\eta k^2}\frac{\hat{D}^2\kappa^2}{1+\kappa^2}\right]. \quad \text{(V.5)}$$

The first term in the brackets in (V.5) corresponds to energy straggling and the second term is due to ωt diffusion due to scattering.

Now, knowing the equilibrium emittance, one can easily determine the equilibrium energy spread and bunch length, relying on equation (III.56):

$$< \left(\Delta\gamma\right)^2 >= \frac{\omega Q_S}{\eta}\varepsilon_S \quad \text{and} \quad < \tau^2 >= \frac{\eta}{\omega Q_S}\varepsilon_S . \quad \text{(V.6)}$$

C. Equilibrium transverse emittances

In order to calculate the scattering rates of transverse emittances, one can use the general expressions (III.33), (III.34), (III.35), and (III.40), where the helix radius, a, is a function of total momentum, p. Both the angle and energy scattering will contribute to the growth of transverse amplitudes. Calculating the growth rate due to momentum jumps along the x_2 direction, we have to take into account that this axis is not perpendicular to the particle total momentum direction, but makes an angle with it whose tangent is $\kappa = p_\perp / p_z$; thus we find:

$$k^2 (a_\pm^2)'_{sc} = \frac{1/\left(1+\kappa^2\right)}{\left(\alpha_+ - \alpha_-\right)^2}\{\frac{1}{2}\left[1 + \frac{Q_\pm^2}{\alpha_\pm^2}(1+\kappa^2)^3\right]\frac{d\theta_{sc}^2}{dz} + \frac{\kappa^2}{\gamma^2\beta^4}\left[1+\sqrt{1+\kappa^2}\hat{D}\alpha_\mp\right]^2\frac{d}{dz}\left(\delta\gamma\right)^2\}. \quad \text{(V.7)}$$

Applying Langevin's balance equations

$$a_\pm^2 = -\Lambda_\pm a_\pm^2 + (a_\pm^2)'_{sc}, \quad \text{(V.8)}$$

we find the following expressions for the equilibrium normalized transverse emittances;

$$\left\langle I_\pm \right\rangle = \varepsilon_\pm = \frac{\Gamma_\pm}{4kQ_\pm}\frac{m_e}{m_\mu\beta}\frac{\Lambda/\Lambda_\pm}{(1+\kappa^2)^{5/2}}, \quad \text{(V.9)}$$

where

$$\Gamma_{\pm} \equiv \frac{(Z+1)[\alpha_{\pm}^2 + (1+\kappa^2)^3 Q_{\pm}^2] + \kappa^2 \left[\alpha_{\pm} - \left(1+\kappa^2\right)^{\frac{3}{2}}\right]^2 (\gamma^2+1)/2log}{\alpha_{\pm}^2 + (1+\kappa^2)\hat{D}^{-1}}. \quad \text{(V.10)}$$

VI. NUMERICAL EXAMPLE OF A HELICAL CHANNEL

Table 1 shows a numerical example of a helical cooling channel using the equations derived in earlier sections. The beam momentum of 100 MeV/c is low compared to the 200 MeV/c of earlier studies in order to attain the best transverse and longitudinal equilibrium emittances as well as to shorten the beam path and reduce the integrated energy loss in the absorber. A rather tight helix ($\kappa \approx 1$) has been chosen in this calculation to moderate the dispersion required for balanced cooling. Lower dispersion improves beam stability and reduces the contribution of energy spread to the radial beam size, the straggling contribution to equilibrium transverse emittances due to dispersion (to about 6%), and the angle scattering contribution to the longitudinal emittance (to 33 %). Note that the calculated 6D emittance may not be a minimum, although further optimization has yet to improve the estimated equilibrium values significantly. The cooling effect in this calculation in terms of reduction of the 6D emittance is 5×10^5. The total energy loss in absorber is about 1.12 GeV. For a channel of continuous dense hydrogen gas with 14 MeV/m of energy loss, this implies a 6D cooling channel length, $L = \frac{1.12}{.014} / \sqrt{1+\kappa^2} = 56$ m.

TABLE 1. Estimated parameters of a helical 6D cooling channel

Parameter	*Unit*	*Initial*	*Middle* [****)]	*Final*
Beam momentum, p [*)]	MeV/c	100	100	100
Solenoid field, B	T	3.5	8	14
Cyclotron wave length, $\lambda_c = 2\pi / k_c$ [*)]	m	0.60	0.26	0.14
Helix period, $\lambda = 2\pi / k$	m	1	0.44	0.22
Helical magnet inner radius	cm	30	12	7
Transverse field at magnet	T	1.7	4.2	7.0
Transverse field at beam center	T	0.7	1.6	3.0
Helix quadrupole gradient	T/m	1.2	7.5	20
Helix orbit radius, a [*)]	cm	15	6	3
Dispersion, D	cm	37	15	7.5
Transverse tunes, Q_+ / Q_-		0.94/0.57	0.94/0.57	0.94/0.57
Transverse beta functions, β_+ / β_-	cm	16/26	6/10	3.2/5.2
Accelerating rf field amplitude	MV/m	40	40	40
Frequency, f=$\omega/2\pi$	GHz	0.2	0.8	1.6
Absorber energy loss rate dE/ds	MeV/m	14	14	14
6D cooling decrement length, Λ^{-1}	m	4	4	4
Individual decrement lengths	m	12	12	12
Synchrotron beta function, β_s	m	0.95	0.47	0.32
Synchrotron tune, $Q_s = 1/\omega\beta_s$		0.25	0.12	0.08
Synchrotron admittance, I_a	cm	3.0	0.37	0.14
Synchrotron emittance, ε_s	cm	1.5 [**)]	0.15 [**)]	3.10^{-2} [***)]
Relative momentum spread	%	7.5 [**)]	3 [**)]	2 [***)]
Bunch length	cm	30 [**)]	7.5 [**)]	1.1 [***)]
Beam width, Δa	cm	3 [**)]	0.56 [**)]	0.15 [***)]
Transverse emittances, $\varepsilon_+ / \varepsilon_-$	cm x rad	1.7/1.7 [**)]	0.2/0.2 [**)]	$(1/3)10^{-2}$ [***)]
Beam widths, σ_1 / σ_2	cm	8/5 [**)]	1.8/1.1 [**)]	0.45/0.28 [***)]

[*)] reference orbit
[**)] maximum deviation from reference orbit
[***)] rms equilibrium value
[****)] at the beginning of the 0.8 GHz section

VII. DISCUSSION

The initial low momentum muon beam with relatively small momentum spread (7.5 %) in the example above could be obtained using a short helical channel with an absorber but no rf. This possibility was proposed and treated previously [17]. Using emittance exchange in this precooling helical channel, all the cooling power of the absorber (with or without wedges) can be taken from the transverse coordinates and concentrated on the longitudinal one to cool the energy spread. Maintaining the transverse emittances, or even by allowing some increase in them for more reduction of energy spread, it is possible to decrease the absolute energy spread a factor of 10 or more before the bunch length is increased significantly. Then, the beam can be captured and bunched by an rf field and injected into the basic cooling channel described by Table I. In this way, the total 6D emittance reduction factor could exceed 10^6. The estimated length of such a deceleration and capture section is less than 25 m.

The example channel assumes smaller, higher-frequency rf cavities will be used when the beam dimensions have been cooled enough to allow them. Reduced transverse dimensions imply that the desired strength of the magnetic fields would be easier to achieve. Higher frequencies make it easier to achieve the desired rf gradients. Short adiabatic helical transition sections would be used to match one stage to the next.

In order to optimize the rf cavity acceptance, each cavity axis could be centered on and aligned with the periodic orbit as the beam wound around the axis of the solenoid, perhaps with the rf waveguides passing through the gap in the helical dipole coil. The large aperture magnets and rf cavities for the 200 MHz stage may be a serious technical challenge and future studies will be toward replacing the initial stage with precooling sections to reduce the beam size. The

precooling under consideration involves transverse cooling with a helical quadrupole section and longitudinal cooling in a short helical dipole section without rf.

The estimated cooling channel length of 56 m for a bunched muon beam of 100 MeV/c assumes that the channel contains rf cavities that operate while filled with dense hydrogen gas. At 50 atmospheres and 77 K, hydrogen gas density is about 21.5% of liquid hydrogen and the corresponding dE/ds for muons with 100 MeV/c momentum, or 46 MeV kinetic energy, is about 14 MeV/m. In this case, the rf cavities must provide sufficient gradient to compensate for $\frac{dE}{dz} = \frac{dE}{ds}\sqrt{1+\kappa^2}$ =20 MeV/m energy loss and provide sufficient rf bucket area for longitudinal beam stability. Thus an average accelerating gradient of around 40 MeV/m is required.

The project by Muons, Inc. and IIT presently underway at Fermilab to develop high-gradient pressurized rf cavities is designed to explore the use of hydrogen and helium gas up to more than 100 atmospheres pressure at temperature down to 77 K. Surface gradients of 80 MV/m for stable operation have been achieved at 800 MHz with 20 μs pulses in hydrogen at 17 atmospheres at liquid nitrogen temperature using molybdenum electrodes. Scaling from the measured Paschen curve data from Lab G, hydrogen gas itself at 50 atmospheres and 77K will support gradients up to 330 MV/m. Future proof-of-principle tests include operation in strong magnetic fields and in intense ionizing radiation. Providing sufficient power is also a necessary condition for high gradient cavities. A scheme has been investigated that implies that 50 MV/m could be generated at 200 MHz using cold copper pillbox cavities for the short pulses required for a neutrino factory or muon collider using pulse compression techniques [32,33].

A cooling channel based on the use of helical magnets and a continuous homogeneous absorber offers advantages compared to other designs. One important advantage is that the cooling system can be described relatively simply with a time-independent, beam-path-

independent Hamiltonian that does not depend on z. Thus the stability and evolution of the beam as it cools can be understood using well-established analytical linear and perturbative non-linear techniques. The next steps in the development of the concepts presented here include simulations to verify the linear and non-linear aspects of the beam dynamics and to continue the experimental investigations to the point that a complete, realistic 6D cooling channel can be designed, prototyped, and built. This concept and particular example are being developed and simulated by Muons, Inc. and the Thomas Jefferson National Accelerator Facility [34]. A description of the project and a preliminary exposition of the ideas presented in this paper were first reported at the Mt. Fuji, Japan cooling workshop [35].

VIII. CONCLUSIONS

A magnetic channel filled with continuous absorber without special edge shaping can be used for emittance exchange cooling of the 6D emittance of a muon beam. This is true for any magnetic arrangement where higher momentum corresponds to a longer path length in a homogeneous absorber and therefore larger ionization energy loss.

The dynamical properties of an attractive example of such a channel have been investigated in some detail, where a solenoidal field is combined with a helical field to provide superior 6D cooling. The continuous nature of the magnetic fields and their helical invariance allows periodic orbits to be found and their stability and cooling properties to be completely analyzed. We have shown that a continuous, homogenous absorber using high-gradient hydrogen-gas-filled rf cavities could provide exceptional 6D cooling in a rather short channel.

Six-dimensional cooling using a homogeneous absorber may be a way to achieve the beam brightness needed for a muon collider. If engineering studies and simulations bear out this prediction, the case for a muon collider as a future energy frontier machine will be strengthened.

Recent discoveries have made a neutrino factory an attractive physics opportunity. The 6D cooling suggested here could provide a neutrino factory with superior performance and reduced costs.

IX. APPENDIX: Hamiltonian framework and canonical relationships

Hamilton's method provides some important relationships of beam dynamics in a magnetic field (or a stationary electromagnetic field). It is based on the introduction of a Hamiltonian with corresponding equations of motion. An ordinary Hamiltonian form is the energy function

$$\hat{E} = \sqrt{p^2 + m^2} + A_o = \sqrt{(\vec{P} - \vec{A})^2 + m^2} + A_o ,$$

with equations of motion

$$\dot{\vec{P}} = -\frac{\partial}{\partial \vec{r}} \hat{E}(\vec{P}, \vec{r}, t),$$

and

$$\dot{\vec{r}} = \frac{\partial}{\partial \vec{P}} \hat{E} .$$

In the case of a particle beam transported along a fixed direction z, it is convenient to consider z as a time argument, while the time t can be treated as one of three independent coordinates x, y, t. Hamilton's function and equations of motion in this representation can be quickly derived using the covariant equation for the wave function $\Psi(\vec{r}, t)$, or the relativistic Schroedinger equation:

$$\left[(\hat{E}+A_o)^2-(\hat{\vec{P}}+\vec{A})^2-m^2\right]\Psi=0,$$

where

$$\hat{E}=i\hbar\frac{\partial}{\partial t}\text{ and }\vec{P}=-i\hbar\vec{\nabla}$$

are the time and space components of 4-vector momentum as a quantum operator. In the quasiclassical limit, this equation can be rewritten, optionally, in two possible forms:

$$i\hbar\frac{\partial}{\partial t}\Psi=\left[\sqrt{(\hat{\vec{P}}+\vec{A})^2+m^2}-A_o\right]\Psi\equiv H_t\Psi,$$

with equations of motion

$$\dot{\vec{P}}=-\frac{1}{i\hbar}[H_t,\vec{P}]=\{H_t,\vec{P}\}\rightarrow-\frac{\partial H_t}{\partial\vec{r}},$$

and

$$\dot{\vec{r}}=\frac{\partial H_t}{\partial\vec{P}},$$

or

$$i\hbar\frac{\partial}{\partial z}\Psi=-\left[\sqrt{(\hat{E}+A_o)^2-(\vec{P}_\perp+\vec{A}_\perp)^2-m^2}+A_z\right]\Psi\equiv H_z(\vec{P}_\perp,\vec{\rho},\hat{E},t,z)\Psi \qquad \text{(IX.1)}$$

with equations of motion

$$\vec{P}'_\pm=-\frac{\partial}{\partial\vec{\rho}}H_z$$

and

$$\vec{\rho}'=\frac{\partial}{\partial\vec{P}_\perp}H_z$$

$$\hat{E}' = -\frac{1}{i\hbar}[H_z, \hat{E}] = \frac{\partial H_z}{\partial t}, \quad t' = -\frac{\partial}{\partial \hat{E}} H_z .$$

Thus, in the z-representation Hamilton's function coincides with the canonical momentum (with reversed sign) $P_z = p_z + A_z$ taken as function of energy and transverse momentum according to the covariant expression $E^2 - p^2 = m^2$.

For a helical structure, it is convenient to consider particle dynamics in terms of a helical frame (x_1, x_2, z), with

$$x_1 + ix_2 = (x + iy)e^{-ikz} . \tag{IX.2}$$

The new Hamiltonian and equations of motion can be simply found using the wave equation in (IX.1), taking into account that

$$\vec{\nabla}_\perp \equiv \vec{e}_x \frac{\partial}{\partial x} + \vec{e}_y \frac{\partial}{\partial y} = \vec{e}_1 \frac{\partial}{\partial x_1} + \vec{e}_2 \frac{\partial}{\partial x_2}$$

and

$$\vec{P}_\perp = \vec{e}_1 P_1 + \vec{e}_2 P_2,$$

while

$$\frac{\partial}{\partial z}\Psi(x, y, z) = (\frac{\partial}{\partial z} + kx_1 \frac{\partial}{\partial x_2} - kx_2 \frac{\partial}{\partial x_1})\Psi(x_1, x_2, z) .$$

Thus, the new Hamiltonian is:

$$H_h = -\sqrt{(\hat{E} + A_o)^2 - m^2 - (P_1 + A_1)^2 - (P_2 + A_2)^2} + A_z + k(x_2 P_1 - x_1 P_2) \tag{IX.3}$$

This is the so-called helical invariant. Since the components of the vector potential A_1, A_2, A_z are functions of only x_1, x_2 (i.e. ρ and $\psi \equiv \varphi - kz$), the Hamiltonian H_h is conserved for any particle trajectory, together with the energy E (assuming no rf and space charge forces).

Solving the equations of motion in a helical structure, one can find the generalized phases $\Psi_\pm$ and adiabatic invariants (quantum numbers) $I_\pm$ as functions of $x_1, P_1; x_2, P_2; E$. In these variables, the Hamiltonian (IX.3) is a function of only I_+, I_-, and E:

$$I'_\pm = \frac{\partial}{\partial \psi_\pm} H_h(I_+, I_-, E) = 0$$

and

$$\psi'_\pm = \frac{\partial}{\partial I_\pm} H_h(E, I_+, I_-) = kQ_\pm(E, I_+, I_-) = const\,. \tag{IX.4}$$

The energy E, being a global invariant in a magnetic field, is not redefined, but there should appear a new time variable $\hat{t}$ as a canonical phase with a constant rate:

$$\hat{t}' = -\frac{\partial}{\partial E} H_h(E, I_+, I_-) = const\,, \tag{IX.5}$$

while the time t on a particle trajectory can be considered as a function of all the "new" variables including $\hat{t}$ and E. There is a set of differential relationships between the "new" and "old" canonical variables [36]. For our situation, the important relationships are:

$$\frac{\partial I_\pm}{\partial \bar{P}_\perp} = \frac{\partial \bar{\rho}}{\partial \psi_\pm} \tag{IX.6}$$

and

$$\frac{\partial I_\pm}{\partial E} = -\frac{\partial t}{\partial \psi_\pm}\,. \tag{IX.7}$$

These can be simply proved comparing the Poisson brackets $\{I_\pm, \vec{\rho}\}$ and $\{I_\pm, t\}$ in terms of "old" and "new" variables.

In order to find the dynamical sense of $\hat{t}$, one has to integrate the equation

$$t' = \frac{1}{\beta_z} = \frac{\sqrt{1 + (\vec{\rho}')^2}}{\beta}$$

along a solved particle trajectory. The inverse particle velocity β_z^{-1} can be represented as

$$\beta_z^{-1} =< \beta_z^{-1} > + \tilde{\beta}_z^{-1},$$

where $\tilde{\beta}_z^{-1}$ oscillates as a function of ψ_+, ψ_-:

$$< \tilde{\beta}_z^{-1} >= 0.$$

Note that $< \beta_z^{-1} >= 1/ < \beta_z >$.

If we introduce the waving fraction of time, $\tilde{t}$, as

$$t =< t > + \tilde{t}(\psi_+, \psi_-), < \tilde{t} >= 0,$$

where

$$\tilde{\beta}_z^{-1} = \tilde{t}' = k(Q_+ \frac{\partial}{\partial \Psi_+} + Q_- \frac{\partial}{\partial \Psi_-})\tilde{t} \quad ,$$

then the variable $\hat{t}$ can be identified as

$$\hat{t} = t - \tilde{t}(\psi_+, \psi_-).$$

This can be proved by comparing equation (IX.5) to the equation for the original time:

$$t' = -\left(\frac{\partial}{\partial E} + \frac{\partial I_+}{\partial E}\frac{\partial}{\partial I_+} + \frac{\partial I_-}{\partial E}\frac{\partial}{\partial I_-} \right) H_h(E, I_+, I_-) = \hat{t}' + kQ_+ \frac{\partial t}{\partial \psi_+} + kQ_- \frac{\partial t}{\partial \psi_-}.$$

Note the important relationships which follow from equations (IX.4) and (IX.5):

$$\frac{\partial}{\partial I_\pm} \frac{1}{< \beta_z >} = -k \frac{\partial}{\partial E} Q_\pm . \qquad \text{(IX.8)}$$

These show that the so-called slippage factors, i.e. emittance-related dispersion of the translation velocity $< \beta_z >$, are simply proportional to the chromaticity of particle tunes [20,21].

To determine the time t as function of "new" variables $(a_\pm, \psi_\pm)$, one has to integrate the equation

$$t' = \frac{1}{\beta_z} = \frac{1}{\beta}\sqrt{1+\left|\hat{x}' + ik\hat{x}\right|^2}$$

along a "solved" particle trajectory. In linear approximation for free particle oscillations near the helical orbit $\vec{a}(p,z)$ we have

$$t' \approx \frac{\sqrt{1+\kappa^2}}{\beta} + \frac{\kappa(ku_1 + u'_2)}{\beta\sqrt{1+\kappa^2}}.$$

To integrate u_1, we have to substitute u_1 as the solution shown in (III.30):

$$\int dz \cdot u_1 = \int (a_+ cos\psi_+ + a\_cos\psi\_)dz = \frac{a_+}{kQ_+} sin\psi_+ + \frac{a_-}{kQ_-} sin\psi_- .$$

Then we obtain equation (III.37). The derivatives $\frac{\partial a_\pm^2}{\partial E}$ can be found using the relationships in (III.31) through (III.34), in which the variables of the rotating frame (x_1, x_1', x_2, x_2') are to be considered as functions of $(x, p_x), (y, p_y)$, and energy E:

$$\hat{x} \equiv x_1 + ix_2 = (x+iy)e^{-ikz},$$

$$\hat{x}' \equiv x_1' + ix_2' = -ik(x+iy)e^{-ikz} + \frac{(p_x + ip_y)e^{-ikz}}{\sqrt{E^2 - m^2 - |\, p_x + ip_y\,|^2}}.$$

Thus, we find

$$\frac{\partial \hat{x}}{\partial E} = 0 \text{ and } \frac{\partial \hat{x}'}{\partial E} = -\frac{\hat{x}' + ik\hat{x}}{p_z^2} E . \qquad \text{(IX.9)}$$

In first approximation, if we neglect the deviations off the equilibrium orbit on the right hand equation in (IX.9), then

$$\frac{\partial x_1'}{\partial E} = 0, \quad \frac{\partial x_2'}{\partial E} = -\frac{ka}{p_z^2} E = -\frac{ka}{E\beta^2}(1+\kappa^2).$$

Now, we can take the derivatives:

$$\frac{\partial}{\partial E}a_{\pm}^2 = 2\frac{x_2' - \alpha_{\mp}k(x_1 - a)}{(\alpha_+ - \alpha_-)^2}\left[-\frac{ka}{E\beta^2}(1+\kappa^2) + \alpha_{\pm}\frac{kda}{\beta dp}\right] = \pm\frac{2a}{E\beta^2}\frac{[\hat{D}\alpha_{\mp} - 1 - \kappa^2]}{\alpha_+ - \alpha_-}a_{\pm}cos\psi_{\pm}. \quad \text{(IX.10)}$$

Finally, using the relationship in (III.28), we find equation (III.39).

Acknowledgments

We are pleased to thank Drs. Boyce, Chattopadhyay, Dylla, Leemann, and Merminga of Thomas Jefferson National Accelerator Facility for the opportunity to continue this research and to investigate with simulations and further analytic calculations the validity of the proposals suggested here. We thank Dr. A. Bogacz for helpful comments. We also thank S. Derbeneva and L. Even for help in preparing the manuscript. Thomas Jefferson National Accelerator Facility is operated by the Southeastern Universities Research Association, Inc. under U.S. Department of Energy Contract DE-AC05-84ER40150. Muons, Inc. is supported in part by SBIR grant DE-FG02-03ER83722.

References

[1] Muon Collaboration, M. M. Alsharo'a *et al.*, Phys. Rev. ST Accel. Beams 6:081001,2003 e-Print Archive: hep-ex/0207031.

[2] A.N. Skrinsky, *Muon Colliders and Neutrino Factories: Basics and Prospects*, APS Fellowship Lecture, Long Beach, CA (2002).

[3] Neutrino Factory and Muon Collider Collaboration, C. M. Ankenbrandt et al., Phys. Rev. ST Accel. Beams 2, 081001 (1999).

[4] S. Geer, *Neutrino beams from muon storage rings: Characteristics and physics potential*, PRD 57, 6989 (1998).

[5] D. Finley and N. Holtkamp eds. *Feasibility Study on a Neutrino Source Based on a Muon Storage Ring*, (Fermilab, Batavia, IL), March 2000. http://www.fnal.gov/projects/muon_collider/nu-factory/fermi_study_after_april1st/

[6] S. Ozaki, R. Palmer, M. Zisman, and J. Gallardo eds. *Feasibility Study-II of a Muon-Based Neutrino Source*, BNL-52623 (2001). http://www.cap.bnl.gov/mumu/studyii/FS2-report.html.

[7] A. N. Skrinsky and V.V. Parkhomchuk, Sov. J. Part. Nucl. 12, p.223-247 (1981).

[8] D. M. Kaplan, *Introduction to Muon Cooling*, http://www.slac.stanford.edu/econf/C010630/papers/M102.PDF.

[9] Invented by Y.S. Derbenev and A. Kondratenko at the Institute of Nuclear Physics in Novosibirsk, the Siberian Snake is a device to be inserted into the lattice of a circular accelerator to preserve the polarization of a proton beam during the acceleration process. See [22] below.

[10] R. P. Johnson et al., *Gaseous Hydrogen and Muon Accelerators*, International Workshop on Hydrogen in Materials and Vacuum Systems, Edited by G. Myneni and S. Chattopadhyay, AIP Conference Proceedings 671, Melville, New York, 2003, pp 328-335.

[11] *Pressurized rf Cavities for Muon Ionization Cooling*, DOE STTR proposal 70255B0I-I (January 2002) by Muons, Inc., (Rolland Johnson PI), with the Illinois Institute of Technology as research partner (Daniel Kaplan subgrant PI). The award, DE-FG02-03ER83722 (July 2002), has been funded at both the Phase I and Phase II levels.

[12] R. E. Hartline, R. P. Johnson, M. Kuchnir, C. M. Ankenbrandt, A. Moretti, M. Popovic D. M. Kaplan, K. Yonehara. *Mark II High-Pressure rf Test Cell Measurements with Molybdenum Electrodes at Lab G*. http://www-mucool.fnal.gov/mcnotes/public/pdf/muc0285/muc0285.pdf

[13] Sanborn C. Brown, *Basic Data of Plasma Physics, The Fundamental Data on Electrical Discharges in Gases, American Vacuum Society Classics*, AIP Press, 1993, p 149.

[14] Proposal to the Rutherford Appleton Lab: An International Muon Ionization Cooling Experiment (MICE**),** The MICE Collaboration. January, 2003 http://hep04.phys.iit.edu/cooldemo/micenotes/public/pdf/MICE0021/MICE0021.pdf.

[15] http://www.muonsinc.com/

[16] http://wwwasd.web.cern.ch/wwwasd/geant4/geant4.html

[17] Y. Derbenev, *Ionization Cooling on Spiral Orbit, complete linear theory*, http://www-mucool.fnal.gov/mcnotes/public/ps/muc0108/muc0108.ps.gz.

[18] V. Balbekov, *Ring Cooler Progress*, http://www-mucool.fnal.gov/mcnotes/public/ps/muc0246/muc0246.ps.gz

[19] Al Garren, Harold Kirk, and Steve Kahn, *Muon Cooling in Gas Filled Cyclotrons*, http://www.fnal.gov/projects/muon_collider/eexchange/workshop03/garren.pdf http://www.physics.ucla.edu/hep/mc/tucson/rc2003.htm

[20] Steve Kahn, Alper Garren, Harold Kirk, *Examining the Garren-Kirk Dipole Cooling Ring with Realistic Fields*, http://www.fnal.gov/projects/muon_collider/eexchange/workshop03/kahn1.pdf

[21] M. Syphers E. Courant, W. Fischer, A. Luccio, F. Mariam, S. Peggs, F. Pilat, T. Roser, S. Tepikian, N. Tsoupas, E. Willen, T. Katayama, K. Hatanaka, T. Kawaguchi, M. Okamura, T. Tominaka, H. Wu, V. Ptitsin, Y. Shatunov, *Helical Dipole Magnets for Polarized Protons in RHIC*, proceedings of the 1997 Particle Accelerator Conf. Available at http://accelconf.web.cern.ch/accelconf/pac97/papers/pdf/3P009.PDF.

[22] Ya. S. Derbenev, A. M. Kondratenko, AIP Conf. Proc., 51, 292 (1979).

[23] E. Willen, M. Anerella, J. Escallier, G. Ganetis, A. Ghosh, R. Gupta, M. Harrison, A. Jain, W. MacKay, A. Marone, J. Muratore, S. Plate, R. Thomas, P. Wanderer and K.C. Wu, *Performance Summary of the Helical Magnets for RHIC*, PAC2003. http://www.osti.gov/dublincore/gpo/servlets/purl/812524-rlkZ2T/native/

[24] V. Balbekov et al., *The Double Flip Cooling Channel (Study II version)* http://www-mucool.fnal.gov/mcnotes/public/pdf/muc0202/muc0202.pdf

[25] A. Artamonov, Ya. Derbenev, and N. Inozemtsev, Sov. Phys. Tech. Phys. 34 (3), 380 (1989).

[26] A. Artamonov, Ya. Derbenev, and N. Inozemtsev, Sov. Phys. Tech. Phys. 34 (4), 495 (1990).

[27] L. D. Landau and E. M. Lifshits, Theoretical Physics v. 8, Electrodynamics of continuous media 1960 QC 518.L23.

[28] A. A. Kolomensky, Sov. Atomic Energy 19, 1511 (1965).

[29] Y. M. Ado and V. Balbekov, Sov. Atomic Energy 39, 40 (1971).

[30] Ya. Derbenev and A. Skrinsky, Sov. Phys. Rev. 1,165 (1981).

[31] http://en.wikipedia.org/wiki/Langevin equation

[32] Alvarez, R. A., *Some Properties of Microwave Resonant Cavities Relevant to Pulse-Compression Power Amplification*, Reviews of Scientific Instrumentation, 1986, v.57, No 10, pp.2481-2488.

[33] Farkas, Z. D., *SLED: A Method of Doubling SLAC's Energy*, Stanford Linear Accelerator Center, Stanford University, Stanford California, May 1974.

[34] *Six-Dimensional Beam Cooling in a Gas Absorber*, DOE SBIR proposal 72180B03-I (January 2003) by Muons, Inc., (Rolland Johnson, PI), with Thomas Jefferson National Accelerator Facility as research partner (Yaroslav Derbenev, subgrant PI). The phase I award is DE-FG02-03ER83722 (July 2003).

[35] Yaroslav Derbenev and Rolland P. Johnson, *Six-dimensional muon beam cooling in a continuous, homogeneous, gaseous hydrogen absorber*, Proc. Int. Conf. On Beam Cooling COOL2003 Mt. Fuji, Japan, May 19-23, 2003 and Nucl. Inst. Meth. A (submitted 2003). Preprint at http://members.aol.com/muonsinc/COOL03_6-d_rev1.pdf.

[36] L. D. Landau and E. M. Lifshits, Theoretical Physics v. 1, Mechanics.